Structures of the Human SPAK and OSR1 Conserved *C*-Terminal (CCT) Domains

Karen T. Elvers,[a,b] Magdalena Lipka-Lloyd,[b] Rebecca C. Trueman,[c] Benjamin D. Bax,[b] and Youcef Mehellou*[a]

[a] Dr. Karen T. Elvers and Dr. Youcef Mehellou
Cardiff School of Pharmacy and Pharmaceutical Sciences
Cardiff University
Cardiff, CF10 3NB, U.K.
E-mail: MehellouY1@cardiff.ac.uk

[b] Dr. Karen T. Elvers, Dr. Magdalena Lipka-Lloyd, and Dr. Benjamin D. Bax
Medicines Discovery Institute
Cardiff University
Cardiff, CF10 3AT, U.K.

[b] Dr. Rebecca C. Trueman
School of Life Sciences
University of Nottingham
Nottingham, NG7 2TQ, U.K.

Supporting information for this article is given via a link at the end of the document.((Please delete this text if not appropriate))

Abstract: STE20/SPS1-related proline/alanine-rich kinase (SPAK) and Oxidative Stress Responsive 1 (OSR1) kinase are two serine/threonine protein kinases that regulate the function of ion co-transporters through phosphorylation. The highly conserved *C*-terminal (CCT) domains of SPAK and OSR1 bind to RFx[V/I] peptide sequences from their upstream With No Lysine Kinases (WNKs), facilitating their activation via phosphorylation. Thus, the inhibition of SPAK and OSR1 binding, via their CCT domains, to WNK kinases is a plausible strategy for inhibiting SPAK and OSR1 kinases. To facilitate structure-guided drug design of such inhibitors, we expressed and purified human SPAK and OSR1 CCT domains and solved their crystal structures. Interestingly, these crystal structures show a highly conserved primary pocket adjacent to a flexible secondary pocket. We also employed a biophysical strategy and determined the affinity of SPAK and OSR1 CCT domains to short peptides derived from WNK4 and NKCC1. Together, this work provides a platform that facilitates the design of CCT domain specific small molecule binders that inhibit SPAK- and OSR1-activation by WNK kinases, and these could be useful in treating hypertension and ischemic stroke.

Introduction

The WNK-SPAK/OSR1 signalling pathway is a key regulator of ion homeostasis in humans.[1] WNK kinases get activated under osmotic stress leading to the phosphorylation, and consequently, the activation of SPAK and OSR1 protein kinases **(Figure 1)**.[2] SPAK and OSR1 kinases bind their upstream WNK kinases via their highly conserved *C*-terminal (CCT) domains, which bind to RFx[V/I] tetrapeptide sequences that are present in the four human WNK isoforms **(Figure 1)**. After binding and phosphorylation by WNK kinases, active SPAK and OSR1 kinases bind the scaffolding Mouse only protein 25 (MO25),[3] of which there are two human isoforms α and β,[4] and as a complex they phosphorylate a number of sodium, potassium and chloride ion co-transporters such as Na-K-2Cl co-transporters 1 and 2 (NKCC1 and 2), Na-Cl co-transporter and K-Cl co-transporter (KCC) **(Figure 1)**.[1] Notably, the binding of SPAK and OSR1 kinases to these ion co-transporters is also mediated by the binding of their CCT domains to RFx[V/I] tetrapeptide motifs on these ion co-transporters akin to the binding of SPAK and OSR1 to WNK kinases **(Figure 1)**. Intriguingly, WNK kinases themselves have CCT-like (CCTL) domains that are have been reported to bind an RFKV peptide,[5] and the structures of CCTL domains from several WNK kinases have been solved by the Structural Genomics Consortium (https://www.thesgc.org/tep/wnk3) and recently reviewed.[6]

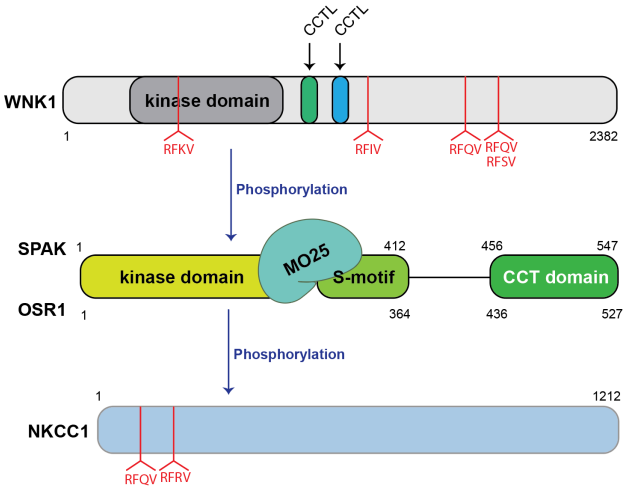

Figure 1. A schematic overview summary of the WNK-SPAK/OSR1-signalling pathway. The four human WNK kinase isoforms and the downstream ion co-transporter substrates of SPAK and OSR1 kinases contain RFx[V/I] tetrapeptide motifs that mediate the binding to SPAK and OSR1 CCT domains, but for simplicity only WNK1 and NKCC1 are shown in this figure.

A number of reports in the literature document mutations of proteins in the WNK-SPAK/OSR1 signalling pathway that result in various human diseases. For instance, genetic mutations in the WNK kinases have been found to lead to familial hyperkalemic hypertension; known as Gordon's Syndrome.[7] Additionally, mutations in two E3 ubiquitin ligases, Cullin 3 (Cul3) and Kelch-Like Protein 3 (KLHL3), which regulate the total protein levels of WNK kinases,[8] have also been found to lead to familial hyperkalemic hypertension.[9] Although most of the studies on the involvement of the WNK-SPAK/OSR1 signalling axis in human diseases have focused on hypertension, there is growing *in vivo*

evidence of the involvement of this signalling pathway in ischemic strokes[10] and breast cancer.[11]
A series of genetically modified WNK, SPAK and OSR1 animal models have shown that inhibition of this signalling pathway leads to a reduction in blood pressure,[12] which offers beneficial outcomes in managing ischemic strokes[13] and treating breast cancer.[11] Although this highlighted the therapeutic potential of inhibiting WNK-SPAK/OSR1 signalling, there have not been any small molecule inhibitors of this signalling cascade that have progressed to clinical studies. Admittedly, there have been various inhibitors of WNK,[14] SPAK and OSR1 kinases,[13, 15] but these had limitations that hindered their further progress. Encouraged by the therapeutic potential of WNK-SPAK/OSR1 signalling inhibitors, this paper focuses on the interaction of SPAK and OSR1 CCT domains with the upstream WNK kinases, which has been shown *in vivo* to be critical for the function of this signalling cascade.[16] In order to facilitate the discovery of small molecule binders of SPAK and OSR1 CCT domains, which inhibit their activation by the upstream WNK kinases, we solved crystal structure of both the human SPAK (hSPAK) and OSR1 (hOSR1) CCT domains.
Determining well defined crystal structures of the conserved CCT domains of hSPAK and hOSR1 seems to have been somewhat problematic. An initial publication in 2007[17] described the hOSR1 CCT domain and identified two pockets, a primary pocket and a secondary pocket. Although an apo structure of hOSR1 CCT

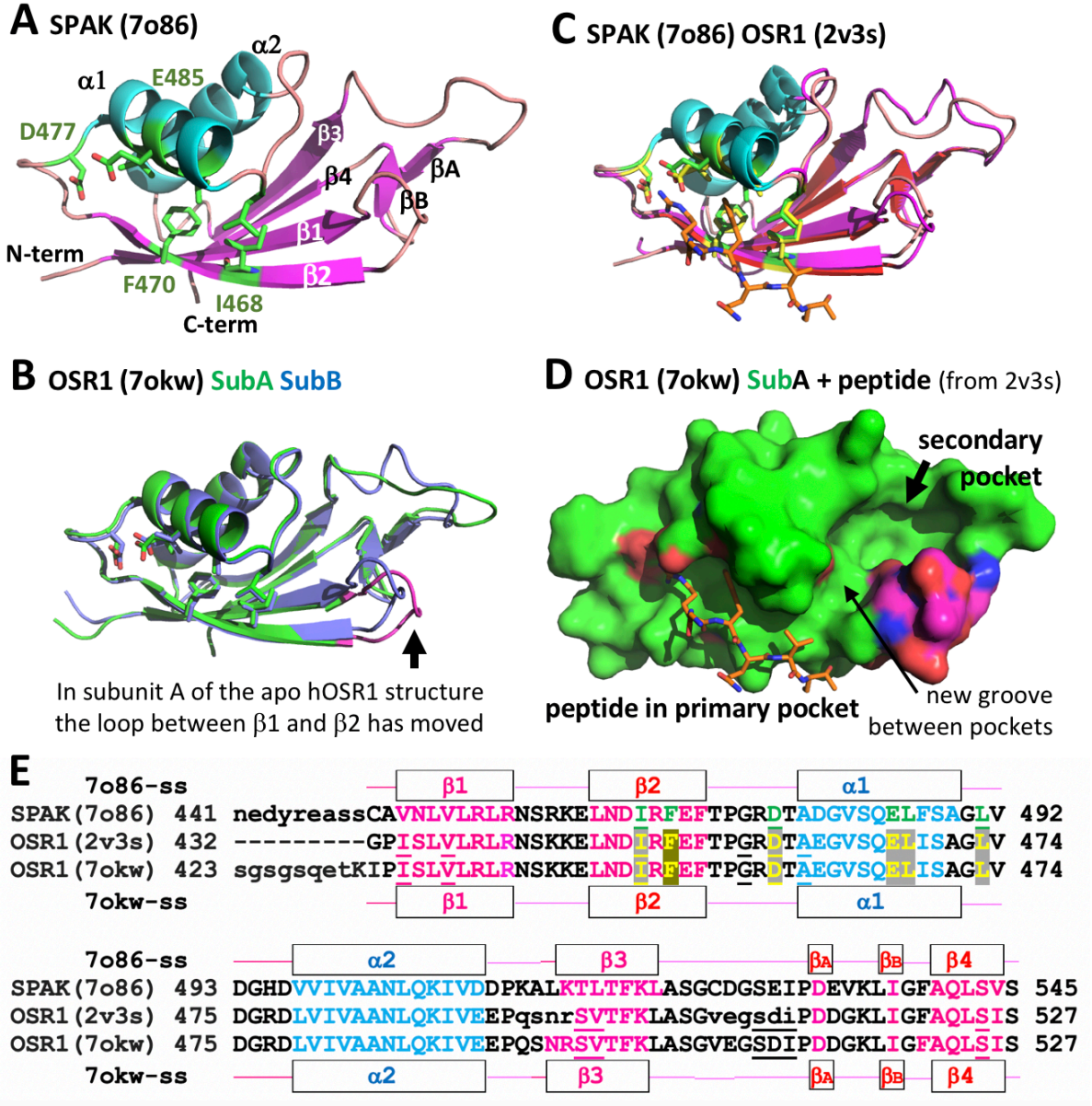

Figure 2. Overview of hSPAK and hOSR1 CCT domain crystal structures. **A**. Subunit A from 1.73Å structure of hSPAK1 CCT domain (pdb code: 7o86) is shown as a cartoon. Six residues involved in the primary peptide binding pocket are shown as sticks with green carbons. **B**. A comparison of subunits A (green/magenta) and subunit B (blue) in the 1.62Å hOSR1 structure (PDB code 7okw). The primary pocket is highly conserved while the loop between β1 and β2 is in different positions in the two subunits. **C**. The 1.70Å structure (PDB code 2v3s) of OSR1 with a six residue peptide (GRFQVT; orange carbons sticks) is shown superposed on A. The six OSR1 residues I450, F452, D459, E467, L468 and L473 are shown as sticks with yellow carbons. **D**. Surface view of subunit A from 1.62Å hOSR1 structure with 6-mer peptide from 2vs3 shown occupying primary pocket. **E**. Protein sequence alignment of the hSPAK CCT domain (7o86) and hOSR1 (2v3s and 7okw) CCT domains. Secondary structural elements are shown above and below the amino-acid sequences. Lower case residues at the *N*-termini of the hSPAK CCT domain (7o86) and hOSR1 (7okw) sequences indicate residues not observed in crystal structures. Lower case residues on the hOSR1 (2v3s) sequence are 494-497 and 507-512 which were disordered in the partial refined apo structure by Villa et al.[17] Underlined residues were disordered in the NMR structure of hOSR1.[33]

domain was described in the paper,[17] it was not deposited with the PDB because of relatively high R-factors (R=0.29, Rfree=0.35). However, a crystal structure of the CCT domain of hOSR1 with a 6-mer peptide was deposited in the PDB (2v3s) and this was the only CCT domain in the PDB prior to this publication.

Results and Discussion

Crystal structures of the hSPAK and hOSR1 CCT domains

To obtain the first crystal structure of hSPAK CCT domain and to deposit an apo hOSR1 CCT domain structure in the PDB, we first designed, cloned, purified and crystallised new hSPAK and hOSR1 CCT constructs comprising amino acids 441-545 for SPAK and amino acids 423-527 for OSR1 (see Experimental Section for amino acid sequences and Supporting Figures S1 and S2). X-ray diffraction of these two crystals gave high resolution structures; a 1.73Å X-ray crystal structure of apo hSPAK CCT (PDB 7o86) and a 1.62Å apo structure of hOSR1 (PDB 7okw; Supporting Table S1 and **Figures 2A** and **2C**). An overview of the two new crystal structures of the hSPAK and hOSR1 CCT domains and their comparison to the only other CCT domain structure in the PDB, the 1.70Å hOSR1 CCT domain (PDB 2v3s) in complex with a 6-mer GRFQVT-peptide[17] is shown in (**Figure 2A**). The primary pocket where the 6-mer peptide binds to OSR1 CCT domain (2v3s) is highly conserved in both subunits of both the apo hSPAK (7o86) and the apo OSR1 (7okw) structures (Supporting Figure S3). In contrast to the highly structurally conserved primary pocket, the secondary pocket, originally identified by Villa et al.[17] is very variable in both of our two new structures (Supporting Figure S3).

Although the loop between the β3 strand and the βA strand, which makes up part of the secondary pocket is highly variable in the structure (**Figure 2** and Supporting Figure S3), the βA-βB region appears to be a rigid and well conserved part of the hSPAK and hOSR1 CCT domain. The βA- and βB-strands are connected by a β-bridge containing just two main-chain hydrogen bonds between D532(hSPAK)/D514(hOSR1) and I537(hSPAK)/519(hOSR1) (these two residues are labelled as β-strands; βA and βB in **Figure 2E**, see also Supporting Figure S3). The side-chain of D532(hSPAK)/D514(hOSR1) also accepts hydrogen bonds from main-chain NHs of V534(hSPAK)/G516(hOSR1) and K535(hSPAK)/K517(hOSR1); the structure between amino acids 532-537 of hSPAK (514-519 of hOSR1) appears quite rigid.

In four out of six hOSR1 and hSPAK subunit structures, the side-chain of R459 (hSPAK)/R441 (hOSR1), the last residue in the β1-strand donates hydrogen bonds to two main-chain carbonyls of K535/517 and L536/518 (Supporting Figure S4). While R441 from the B subunit in the 1.62Å hOSR1 structure makes this usual interaction (with main chain carbonyls of K517 and L518). In the A subunit, an interaction is only observed between the side-chain of R441 and the carbonyl of K517. This move correlates with a change in the size of the secondary pocket,[15a] in the A subunit of the 1.62Å hOSR1 structure (**Figure 2D**). The flexibility of the secondary pocket is a notable feature of the structures and may partially account for difficulties in crystallisation.

Our deposited hOSR1 structure (7okw) and that of hOSR1 reported by Villa *et al.* (2v3s)[17] are very similar in the primary pocket (**Figure 2**), but have differing structures in the secondary pocket region (**Figure 2D** and Supporting Figure S3). The secondary pocket in subunit A in our hOSR1 structure (**Figure 2D**) and the secondary pocket in subunit B in our hSPAK structure

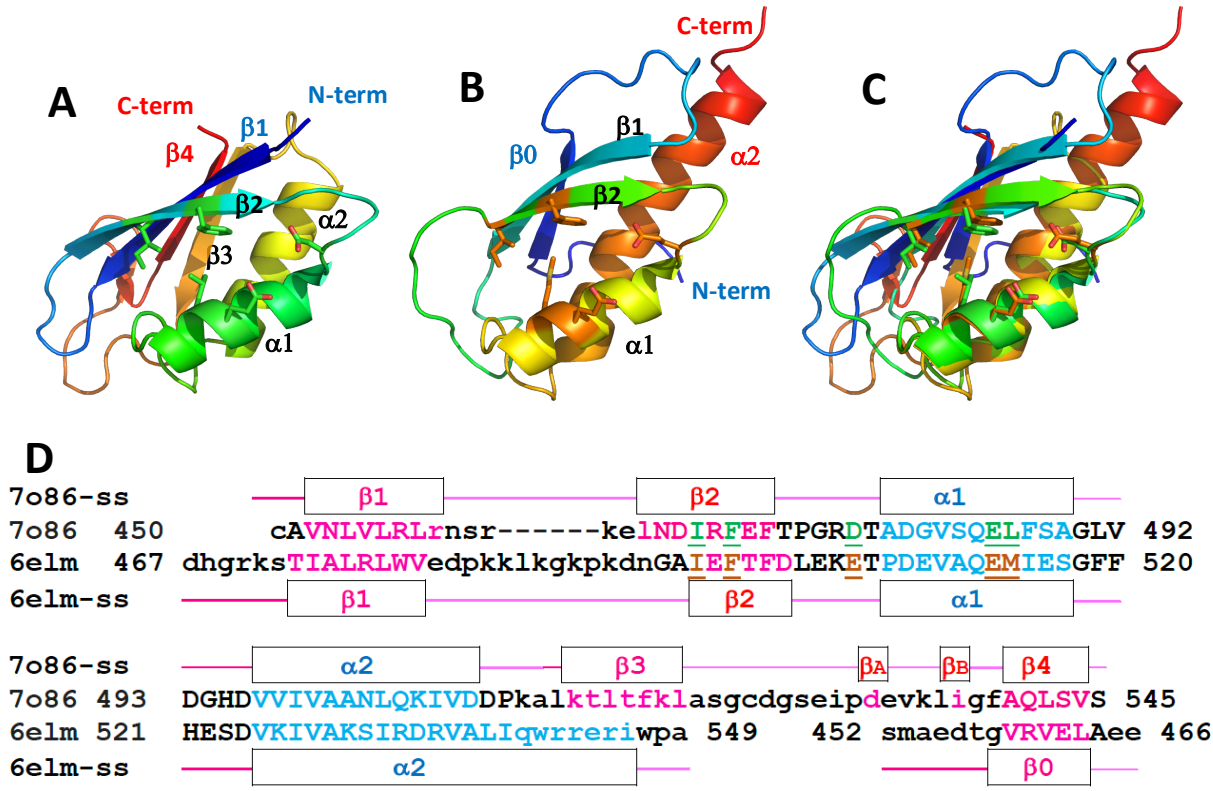

Figure 3. Comparison of the hSPAK CCT domain structure with the CCTL1 domain from WNK2. A. hSPAK CCT domain structure (pdb code 7o86) is shown as cartoon with colour ramp from blue (*N*-term–C450) to red (*C*-term–S545). The four strands in the β-sheet and the two α-helices are labelled as shown on sequence alignment. **B.** WNK2 CCTL1 structure (pdb code 6elm) is shown as cartoon with colour ramp from blue (*N*-term–S452) to red (*C*-term–A549). The three strands in the β-sheet and the two α-helices are labelled as shown on sequence alignment. Note that the β0 strand comes before the β1 strand. **C** comparison of A and B. **D** a structurally based sequence alignment. Uppercase residues superpose-lowercase residues are in different positions in the two structures. Five residues, involved in forming the peptide binding pocket are underlined and coloured. These residues are shown as side-chain sticks in panels A and B.

(Supporting Figure S3) have quite different shapes, at least partly due to a movement of the loop between the β1 and β2 strands (**Figure 2** and Supporting Figure S3).
Although the hSPAK CCT domain structure we have refined and deposited with the PDB (7o86) has reasonable R-factors (R=0.196, Rfree=0.240), the structure has high temperature factors (Supporting Figure S5) in loops in similar positions to the OSR1 'disorderd loops' (see **Figure 2E**). Moreover, it is possible to model a 'domain swapped' dimer[18] into the hSPAK CCT structure (Supporting Figure S5). One possibility could be that the rigid structure centred on the βA and βB strands (**Figure 2**) could be used as part of an allosteric mechanism to define different shapes of the secondary pocket.

Comparison of the hSPAK CCT domain with CCTL domains from WNK kinases

In 2013, the NMR solution structure of an autoinhibitory CCTL domain from WNK1, which associated with a GRFKV peptide, was reported.[5] Although this domain had the conserved primary pocket peptide binding site observed in the hSPAK and hOSR1 CCT domain, the domain lacks the last two strands observed in hOSR1 and hSPAK CCT domains (**Figure 3**). The SGC have now solved crystal structures of number of CCTL domains from WNK kinases (https://www.thesgc.org/tep/wnk3), which all have the basic same fold as that observed by Moon et al.[5] One of these, a well refined 1.1Å structure WNK2 CCTL1domain (PDB 6elm) is compared with the hSPAK CCT domain structure in **Figure 3**. Note that β-strands 3 and 4 from the 1.73Å hSPAK structure are not observed in the WNK2 CCTL1, but a strand in the same position as β4 comes at the *N*-terminus of the domain (we call this strand β0) see **Figure 3**. The primary pocket is conserved between CCT and CCTL domains, but the secondary pocket is not conserved. Differences in the secondary pocket between the CCT domains of hSPAK and hOSR1 and the CCTL domains within WNK kinases may be important in the activation of hSPAK and hOSR1 by WNKs. Interestingly although the 1.1Å structure of the WNK2 CCTL1 domain has excellent R-factors (R = 0.138, Rfree = 0.168), a 1.7Å structure of the same WNK2 CCTL1 with an 18mer RFXV-motif peptide (PDB 6FBK) does not have such good R-factors (R = 0.284, Rfree = 0.334) (https://www.thesgc.org/tep/wnk3).

Analysis of binding properties of hSPAK and hOSR1 CCT domains to WNK kinases

As mentioned above, hSPAK and hOSR1 CCT domains interact with the upstream WNK kinases and the downstream ion co-transporters by binding to RFx[V/I] containing sequences. A number of studies investigated the binding affinities of peptides derived from WNK4 to hSPAK and hOSR1 CCT domains using a range of biophysical assays namely Surface Plasmon Resonance (SPR)[19] and Fluorescence Polarisation (FP).[15a, 16] The binding affinity ranged from one study to another depending on the assay and conditions used (Supporting Table S2). Below, new biophysical assays that employ the Creoptix WAVE system (www.creoptix.com) are described. These assays have the advantage of offering insights into the kinetics of hSPAK and hOSR1 CCT domains binding to an 18-mer RFQV peptide derived from WNK4. Notably, this 18-mer RFQV peptide was the same peptide used in an SPR assay by Vitari et al.[19]
In the first instance, we embarked on measuring the binding affinity of the 18-mer RFQV peptide to hSPAK and hOSR1 CCT domains by labelling the proteins with biotin and immobilising them on a chip while the 18-mer peptide was the analyte, and the binding was evaluated using waveRAPID and traditional multicycle kinetics (**Figure 4**). The results showed that using a 1:1 kinetic model and global fitting, the K_D for the 18-mer peptide at 5 μM was 1.1 μM and 2.5 μM for hSPAK and hOSR1, respectively (**Figure 4A** and **4C**). The K_D value was essentially the same in waveRAPID when the 18-mer peptide, hSPAK and hOSR1 were used at different concentrations (Supporting Figures S6 and S7 and Supporting Table S3). Also, the K_D for the 18-mer was 1.16 and 2.5 μM for hSPAK and hOSR1 respectively with traditional multicycle kinetics (**Figure 4B** and **4D**). These K_D values are comparable to those reported previously (Supporting Table S2)[15a, 15c, 16, 20] using SPR and fluorescence polarisation although most of these studies employed GST-tagged hSPAK and hOSR1 CCT domains, which will be dimeric. This may account for some of the differences observed in values in the literature. In order to verify that the measured binding affinity is a true reflection of the binding of the 18-mer peptide to hSPAK and hOSR1 CCT domains, we subsequently measured the binding affinity of the 18-mer peptide to hSPAK L491A and hOSR1 L473A. The results showed that there was no binding between the WNK-derived 18-mer to hSPAK L491A and hOSR1 L473A (Supporting Figures S8 and S9), and this is in agreement with the previous data obtained for measuring the binding affinity of these hSPAK and hOSR1

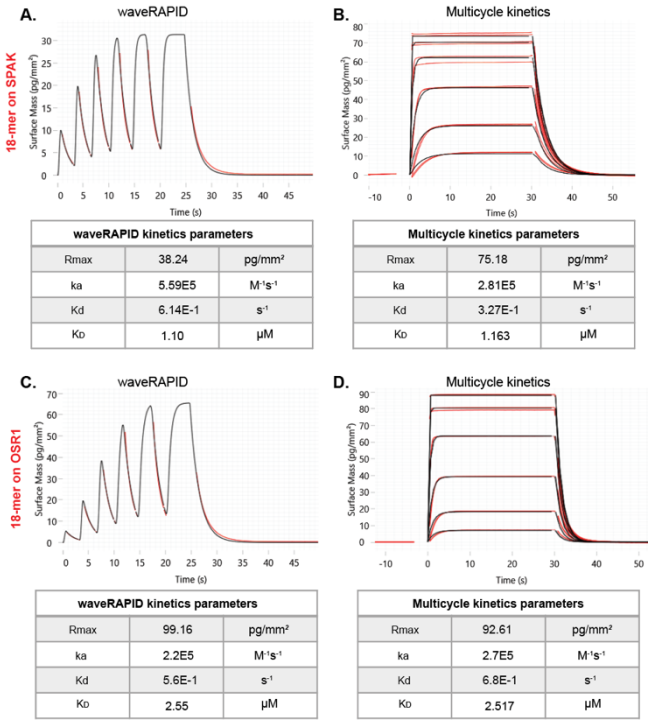

waveRAPID kinetics parameters		
Rmax	38.24	pg/mm²
ka	5.59E5	$M^{-1}s^{-1}$
Kd	6.14E-1	s^{-1}
K_D	1.10	μM

Multicycle kinetics parameters		
Rmax	75.18	pg/mm²
ka	2.81E5	$M^{-1}s^{-1}$
Kd	3.27E-1	s^{-1}
K_D	1.163	μM

waveRAPID kinetics parameters		
Rmax	99.16	pg/mm²
ka	2.2E5	$M^{-1}s^{-1}$
Kd	5.6E-1	s^{-1}
K_D	2.55	μM

Multicycle kinetics parameters		
Rmax	92.61	pg/mm²
ka	2.7E5	$M^{-1}s^{-1}$
Kd	6.8E-1	s^{-1}
K_D	2.517	μM

Figure 4. Comparison of multicycle kinetics with waveRAPID kinetics. Binding was measured for the 18-mer peptide SEEGKPQLVGRFQVTSSK (analyte) to immobilized biotin-hSPAK or biotin-hOSR1 generated with either waveRAPID (**A** and **C**, left panel; 18-mer at 5 μM) or with traditional multicycle kinetics (**B** and **D** right panel; 18-mer at 50 μM 3 fold dilutions). The double-referenced response data (red) are fitted with a one-to-one binding (black lines) with a suitable model in waveControl (model traditional fit). Table summaries of kinetic parameters are shown: Rmax, ka, association rate constant; kd, dissociation rate constant; and K_D dissociation constant.

mutants to the RFQV 18-mer peptide (Supporting Table S2).[16, 19] Subsequently, we attempted measuring the binding affinity of the WNK-derived 18-mer RFQV peptide to hSPAK and hOSR1 CCT domains using the reverse situation where the *N*-terminally biotinylated 18-mer RFQV peptide was immobilised to the streptavidin surface and hSPAK and hOSR1 CCT domains were the mobile analytes. In this case, the binding affinity of OSR1 to the peptide resulted in K_Ds of 2.1 and 6.6 μM using waveRAPID and multicycle methods respectively (**Figure 5B** and **5C**). For hSPAK, there was clearly a more pronounced slow-off rate and/or non-specific binding component. In waveRAPID, this can be seen where the dissociation does not return quickly to baseline (Figure 5A). A K_D of 1.2 μM was determined using a heterogeneous model in which the heterogeneous ligand model supposes two types of differently interacting binding and is able to separate the

two (**Figure 5A**). In multicycle kinetics, the incomplete dissociation of the slow binding component prevents the software fitting a model to the data (data not shown). In this scenario, waveRAPID achieves good data because it has a much lower contact time, which does not allow the slow component time to build up on the surface.

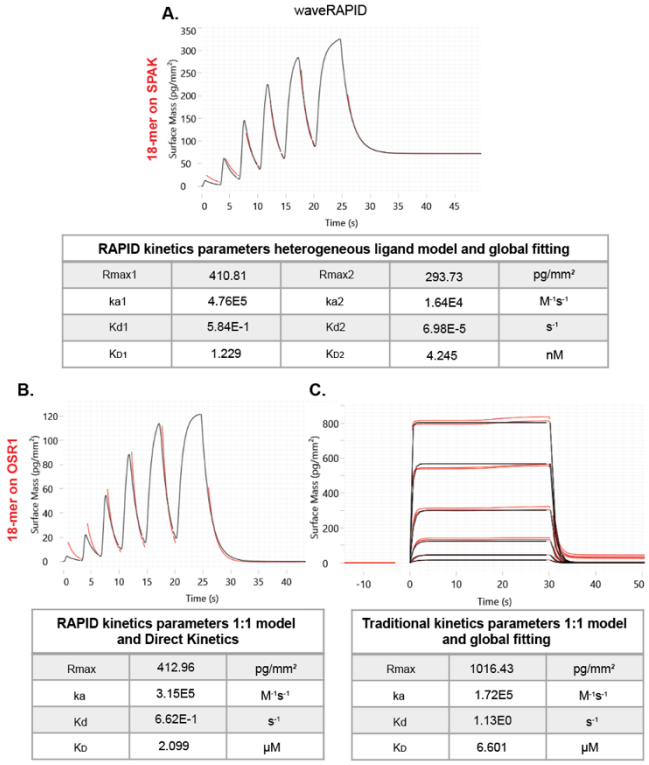

RAPID kinetics parameters heterogeneous ligand model and global fitting				
Rmax1	410.81	Rmax2	293.73	pg/mm²
ka1	4.76E5	ka2	1.64E4	$M^{-1}s^{-1}$
Kd1	5.84E-1	Kd2	6.98E-5	s^{-1}
K_{D1}	1.229	K_{D2}	4.245	nM

RAPID kinetics parameters 1:1 model and Direct Kinetics		
Rmax	412.96	pg/mm²
ka	3.15E5	$M^{-1}s^{-1}$
Kd	6.62E-1	s^{-1}
K_D	2.099	µM

Traditional kinetics parameters 1:1 model and global fitting		
Rmax	1016.43	pg/mm²
ka	1.72E5	$M^{-1}s^{-1}$
Kd	1.13E0	s^{-1}
K_D	6.601	µM

Figure 5. Comparison of traditional kinetic data and estimates with waveRAPID. Binding was measured for cleaved hSPAK and hOSR (analyte) to captured biotin-C_6-SEEGKPQLVGRFQVTSSK generated with either waveRAPID (**A** for hSPAK and **B** for hOSR1) or with traditional multicycle kinetics (**C** for hOSR1). The double-referenced response data (red) are fitted with a binding model (black lines). Here the binding model and fitting are indicated on the Figure. Table summaries of kinetic parameters are shown: Rmax 1 and 2, ka, association rate constant; kd, dissociation rate constant; and K_D dissociation constant.

As well as using the Creoptix WAVE system for measuring the binding affinity of hSPAK and hOSR1 CCT domains to RFQV peptides derived from the upstream WNK kinases, we employed this same strategy for measuring the binding affinity of these CCT domains to RFQV peptides derived from the downstream protein binder NKCC1. Indeed, we used a 19-mer RFQV and its single point mutant 19-mer AFQV peptides derived from the human NKCC1, and the results showed that the wild-type peptides did bind hSPAK and hOSR1 CCT domains in good affinity (5-10 µM) (Supporting Figure S10) while the mutant peptide was unable to bind these CCT doamins (Supporting Figure S11).
Collectively, the Creoptix WAVE method for measuring the binding affinities of the RFQV 18-mer peptide to hSPAK and hOSR1 CCT domains gave values that are comparable to previously reported K_D values. This validates this method as a viable strategy for measuring the binding affinity of the RFQV 18-mer peptide to SPAK and OSR1 CCT domains and highlights the potential of using this assay in screening inhibitors of hSPAK and hOSR1 CCT domains binding to WNK kinases.

Conclusion

In order to facilitate the discovery of SPAK and OSR1 kinase inhibitors, we herein reported the crystal structures of hSPAK and hOSR1 CCT domains. These domains are believed to be critical in the binding of SPAK and OSR1 kinases to their upstream WNK kinases, a process that leads to SPAK and OSR1 activation via phosphorylation by WNK kinases. After SPAK and OSR1 are activated by phosphorylation by WNK kinases, conformational changes and interaction with MO25 are presumed to cause changes in the SPAK and OSR1 CCT domains causing them to preferentially bind to motifs in the downstream ion channels (using the same type of RFx[V/I] CCT domain interaction).
The crystal structures of hSPAK and hOSR1 CCT domains will be a powerful resources in the *in silico* design of new SPAK and OSR1 inhibitors. Additionally, the Creoptix WAVE assay reported in this work is also a powerful technology for screening small molecules that bind SPAK and OSR1 CCT domains, and in deciphering the fascinating regulatory interactions of the proteins with RFx[V/I] motifs from both upstream WNK kinases and downstream ion channels. Collectively, this work provides new resources and tools that will facilitate the discovery of new SPAK and OSR1 inhibitors that have the potential to ultimately improve the lifestyle of patients suffering from hypertension and who are at high risk or have had ischemic strokes.

Experimental Section

Construct design. hSPAK and hOSR1 CCT domain constructs were designed with: (i) an *N*-terminal His tag, (ii) an Avi-Tag (*GLNDIFEAQKIEWHE*) a unique 15 amino acid peptide tag for targeted enzymatic conjugation of a single biotin on the lysine using biotin ligase and (iii) a TEV-cleavage site (**ENLYFQG**). The DNAs for these were synthesised by GenScript (in pUC57). The amino acid sequence of the expressed uncleaved hSPAK construct (residues 441-545 underlined) is: MHHHHHHSS*GLNDIFEAQKIEWHE*SS**ENLYFQG**NEDYREASSCAVNL VLRLRNSRKELNDIRFEFTPGRDTADGVSQELFSAGLVDGHDVVIVAAN LQKIVDDPKALKTLTFKLASGCDGSEIPDEVKLIGFAQLSVS. After cleavage with TEV protease the protein hSPAK CCT domain contains a single additional glycine residue from the tag at the *N*-terminus (G*NEDY*). The amino acid sequence of the human hOSR1 (423-527 underlined) CCT is:HMHHHHHHSS*GLNDIFEAQKIEWHE*SS**ENLYFQG**SGSGSQETKIPIS LVLRLRNSKKELNDIRFEFTPGRDTAEGVSQELISAGLVDGRDLVIVAAN LQKIVEEPQSNRSVTFKLASGVEGSDIPDDGKLIGFAQLSIS. A further two constructs were synthesised by GenScript as above but with point mutations leucine to alanine (in bold and underlined) at amino acid L473 in OSR1 and L491in SPAK.
The amino acid sequence for uncleaved mutated hSPAK construct is: MHHHHHHSS*GLNDIFEAQKIEWHE*SS**ENLYFQG**NEDYREASSCAVNL VLRLRNSRKELNDIRFEFTPGRDTADGVSQELFSAG**A**VDGHDVVIVAA NLQKIVDDPKALKTLTFKLASGCDGSEIPDEVKLIGFAQLSVS and uncleaved mutated hOSR1 is: HMHHHHHHSS*GLNDIFEAQKIEWHE*SSENLYFQGSGSGSQETKIPISLV LRLRNSKKELNDIRFEFTPGRDTAEGVSQELISAG**A**VDGRDLVIVAANL QKIVEEPQSNRSVTFKLASGVEGSDIPDDGKLIGFAQLSIS
Cloning and Expression: hSPAK, hOSR1, hSPAK L491A and hOSR1 L473A CCT domain constructs were subcloned into a pET24a(+) expression vector using standard molecular methods, using OneShot TOP10 Chemically Competent *E.coli* (Invitrogen) and appropriate antibiotics. DNA sequences were confirmed by sequencing (Eurofins). For protein expression, plasmids were transformed into BL21-CodonPlus (DE3)-RIL competent *E.coli* (Agilent Technologies). Cultures was grown at 37°C to an OD_{600} 0.6-0.8 in LB media with kanamycin (50µg/ml) and chloramphenicol (35 µg/ml). Expression was induced by the addition of 0.125 mM isopropyl β-D-1-thiogalactopyranoside (IPTG; Melford Laboratories Ltd), and the culture grown overnight at 20 °C.
Purification of hSPAK-CCT and hOSR-CCT: Uncleaved proteins (hSPAK, hOSR1, hSPAK L491A and hOSR1 L473A CCT doamins) were purified from supernatant of lysed cells, in two steps (at 4°C). 1. Affinity capture on a 5 ml HisTrap FF column in wash buffer [50 mM Tris.HCl pH 7.8, 300 mM NaCl, 5% glycerol and 5 mM imidazole], and eluted with a linear imidazole gradient [50 mM Tris.HCl pH 7.8, 300 mM NaCl, 5% glycerol and 250 mM imidazole]. 2. Size exclusion chromatography (SEC) on a Superdex 16/600 75 pg with SEC buffer [20 mM Tris.HCl pH 7.8, 50 mM NaCl, 1 mM DTT] (see Supporting Figures S1 and S2). Proteins were

concentrated using MWCO 3K PES centrifugal concentrators (Pall Corporation) at 4,700*g* at 10°C before loading on the SEC column. Uncleaved protein eluted as a single peak. Fractions were pooled, concentrated and subsequently quantified by Bradford assay. SDS-PAGE (16% Tris-Glycine; Invitrogen) was used for analysis at each stage.

Modifications post purification. *i. hSPAK and hOSR1 for crystallisation.* hSPAK and OSR1 CCT domains were cleaved at a Q/G site with Tobacco Etch Virus (TEV) Protease to remove the *N*-terminal 6xHis (underlined) and AviTag (bold) (MHHHHHHSS**GLNDIFEAQKIEWHE***SSENLYFQ*/G). The cleaved tag was removed by incubation with 0.5 ml Super Cobalt NTA Agarose Affinity Resin (Generon) and the flow through containing hSPAK was loaded on and run on a Superdex 16/600 75pg SEC column pre-equilibrated with SEC buffer [20 mM Tris.HCl pH 7.8, 50 mM NaCl, 1 mM DTT]. Fractions were pooled and concentrated using Cerocon (SWISSCI) 0.5 ml concentrator at 3 kDa MWCO. They were quantified by Bradford assay (see Supporting Figures S1 and S2).

ii. hSPAK and hOSR1 as analytes for surface-based biophysical measurement of binding kinetics. Both proteins were cleaved with TEV as above, but the final SEC was run using HBS EP buffer [10 mM HEPES pH7.4, 150 mM NaCl, 3 mM EDTA, 0.005% Tween20].

iii. Biotinylated hSPAK and hOSR1 and alanine mutations as ligands for binding kinetics. Enzymatic biotinylation with *E. coli* biotin ligase (BirA) was carried out to specifically biotinylate the lysine residue in the AviTag sequence GLNDIFEAQ**K**IEWHE. Briefly, 750 µg of purified uncleaved hSPAK or hOSR CCT domains were mixed with 50 µl of SuperMix (containing ATP and D-biotin, Avidity, LLC) and 5 µg of BirA (Avidity, LLC), to a final volume of 500 µL buffer [20 mM Tris.HCl pH 7.8, 50 mM NaCl, 1 mM DTT]. The reaction was incubated overnight at 4 °C with mixing. The free biotin and BirA ligase were removed from the final biotinylated proteins by size exclusion in HBS EP buffer. Final fractions containing biotinylated protein were concentrated and quantified by Bradford assay and termed biotin-hSPAK and biotin-hOSR1.

Crystallisation, data collection and structure determination of CCTs. Cleaved hSPAK-CCT (1.4 mg/ml) was crystallised using a Mosquito liquid handling robot (TTP Labtech) in a SWISSCI 3 lens sitting drop plates, using a drop ratio of 150 nls protein (in 20 mM Tris.HCl pH 7.8, 50 mM NaCl, 1 mM DTT) and 50 nls well. The hSPAK CCT domain crystal structure reported in this paper was from a crystal grown against well of Morpheus A5 (30 mM $MgCl_2$, 30 mM $CaCl_2$, 50 mM sodium HEPES, 50 mM MOPS pH 7.5, 20% v/v PEG 500 MME, 10% w/v PEG 20000) at 6 °C. The crystal used for data collection was picked in a loop and plunged into liquid nitrogen. Data were collected on beam-line i03 at Diamond Light Source. The 1.73Å dataset (Supporting Table S1) was autoprocessed with DIALS[21] run via the xia2 autoprocessing pipeline.[22] The dataset contains some 3600, 0.1 degree images (360 degrees of data); examination of merging statistics by batch did not show any major variation with batch. The Rmerge in low resolution shells is around 6%.

The structure was solved by molecules replacement with phaser [23] using the OSR1 CCT (PDB code: 2v3s, residues 434-526 of subunit A -some side-chains trimmed). The structure was refined with Refmac5[24] and phenix.refine [25] and rebuilt in coot.[26] Coordinates have been deposited with the PDB (pdb code: 7o86).

Cleaved hOSR1 CCT domain (1.89 mg/ml) was crystallised using a Mosquito liquid handling robot (TTP Labtech) in a SWISSCI 3 lens sitting drop plates, using a drop ratio of 150 nls protein (in 20 mM Tris.HCl pH 7.8, 50 mM NaCl, 1 mM DTT + compound 1 at 1 mM and 10%DMSO) and 50 nls well. The OSR1 crystal structure reported in this paper was grown against well of Morpheus A8 (30 mM $MgCl_2$, 30 mM $CaCl_2$, 50 mM sodium HEPES, 50 mM MOPS pH 7.5, 25% v/v MPD; 25% PEG 1000; 25% w/v PEG 3350) at 6 °C.

The crystal used for data collection was picked in a loop and plunged into liquid nitrogen. Data were collected on beam-line i04 at Diamond Light Source. The 1.62Å dataset (Supporting Table S1) was autoprocessed with Autoproc/STARANISO.[27] The diffraction limits of ellipsoid fitted to diffraction cut-off surface were 1.598, 1.763 and 1.768Å. The structure was solved by molecules replacement with phaser[23] using the OSR1 CCT (PDB code: 2v3s, residues 434-526 of subunit A -some side-chains trimmed). The structure was refined with Refmac5[24] and phenix.refine[25] and rebuilt in coot.[26] Coordinates have been deposited with the PDB (pdb code: 7okw).

Structure analysis. Secondary structures were calculated with DSSP[28] as implemented on the web server https://swift.cmbi.umcn.nl/gv/dssp/.[29] The only helices shown in Figures are α-helices. Buried area between different subunits in crystals were analysed with the program PISA[30] at the EBI (https://www.ebi.ac.uk/pdbe/pisa/). The nine amino acids at the *N*-terminus of the peptide modelled in Supporting Figure 3L, with sequence E**EGKPQLVG,** were initially modelled as a polyproline helix based on residues A1-A9 from pdb code 1x1k, replacing side-chains.[31] The docked helix was energy minimised onto the structure using Maestro (Schrödinger Release 2020-2: Maestro, Schrödinger, LLC, New York, NY, 2021).

Surface-based biophysical measurement of binding kinetics. Grated-Coupled Interferometry (GCI) experiments were performed on a Creoptix WAVE system (Creoptix, AG) using 4PCH STA WAVE sensor chips (polycarboxylate surface, streptavidin coated). Chips were conditioned with borate buffer (100 mM sodium borate pH9, 1 M NaCl; Xantec). Biotin-hSPAK, biotin-hOSR1, biotin-hSPAK L491A and biotin-hOSR1 L473A were directly immobilized onto the sensor chip by injection onto the surface in HBS EP [10 mM HEPES pH7.4, 150 mM NaCl, 3 mM EDTA, 0.005% Tween20] buffer at 10 µg/ml at a flowrate of 10 µl/min. The final surface density for the biotin-hSPAK, biotin-hOSR1 and alanine mutations was about 1000 pg/mm^2. The biotinylated 18-mer peptide (Biotin-C_6-SEEGKPQLVGRFQVTSSK) was purchased from (GL Biochem, Shanghai Ltd). The density of the biotin-peptide was controlled to about 400 pg/mm^2. Kinetic analyses were performed at 25°C using, **(a)** waveRAPID (Repeated Analyte Pulses of Increasing Duration - multiple short pulses of the analyte at a single concentration but of increasing durations.[32] The experiments were carried out at flow rate of 100 µl/min. Briefly, 122 µL of samples were applied to the immobilised surface and reference for 25 s total injection duration, followed by a 300s dissociation with assay buffer and **(b)** traditional multicycle kinetics where the analyte is introduced at increasing concentrations with injection of uniform duration. The experiment was carried out at flow rate of 120 µl/min. 110 µL of the analytes were injected for 30s, followed by a 300s dissociation for 18-mer peptide and hOSR1 and 2000s dissociation for hSPAK with assay buffer. The analyses were measured with two scenarios.

i. Immobilised biotin-hSPAK or biotin-hOSR1, or biotin-hSPAK L491A or biotin-hOSR1 L473A as 'ligands' with binding kinetics of unbiotinylated 18-mer peptide (SEEGKPQLVGRFQVTSSK, GL Biochem, Shanghai Ltd).

ii. The inverse set up, immobilised biotin 18-mer peptide as the 'ligand' and the binding kinetics of cleaved hSPAK and cleaved hOSR1 were analysed.

The following concentrations of analytes were used.

i. Immobilised hSPAK or hOSR1 CCT domains: In waveRAPID; the 18-mer peptide concentration was 2, 5, 10 or 20 µM. In multicycle kinetics, the 18-mer was serially diluted 3-fold using assay buffer for a six point dose curve (50 µM, 17 µM, 5.5 µM, 1.8 µM, 0.6 µM, 0.2 µM).
ii. Immobilised 18-mer peptide: In waveRAPID when biotinylated peptide was captured onto the chip the kinetics of cleaved hOSR1 and hSPAK CCT domains at 2 µM. In multicycle kinetics cleaved hOSR1 and hSPAK CCT domains were serially diluted 1:3 using assay buffer for a six point dose curve (25 µM, 8.3 µM, 2.8 µM, 925.9 nM, 308.6 nM, 102.9 nM).

The kinetics of the 19-mer NKCC1 peptide (LGPTPSQSRFQVDLVSENA, GL Biochem, Shanghai) and the R to A mutated peptide (LGPTPSQS**A**FQVDLVSENA) were also measured using waveRAPID. Biotin-hSPAK and biotin-hOSR1 were immobilised to a surface density of 2500 pg/mm^2. The experiments were carried out at flow rate of 100 µl/min. The 19-mer peptides at 5 and 10µM were applied to the immobilized surface and reference channel for 25s total injection duration, followed by a 300s dissociation with assay buffer. In all experiments, blank injections were used for double referencing and a DMSO calibration curve for bulk correction. Analysis and correction of the obtained data were performed using the Creoptix WAVE control software 4.2 (correction applied: X and Y offset; DMSO calibration; double referencing). One-to-one binding and heterogeneous models were used with a suitable fitting model.

Acknowledgements

We thank Fabio Andres and Edward FitzGerald (Creoptix AG, Wädeswil, Switzerland) for their excellent support in the analysis of the Creoptix WAVE data and suggestions for additional experiments. We acknowledge the Diamond Light Source for beamtime (proposal MX20147) and the staff of beamlines I03 and I04 for assistance with diffraction data collection. The work was funded by a Medical Research Council grant (Ref. 518455) awarded to Y.M. and B.D.B.

Keywords: SPAK • OSR1 • Kinase • Crystal structure • Inhibitor

[1] a) D. R. Alessi, J. Zhang, A. Khanna, T. Hochdorfer, Y. Shang, K. T. Kahle, *Sci. Signal.* **2014**, *7*, re3; b) J. Hadchouel, D. H. Ellison, G. Gamba, *Annu. Rev. Physiol.* **2016**, *78*, 367-389.
[2] A. C. Vitari, M. Deak, N. A. Morrice, D. R. Alessi, *Biochem. J.* **2005**, *391*, 17-24.

[3] B. M. Filippi, P. de los Heros, Y. Mehellou, I. Navratilova, R. Gourlay, M. Deak, L. Plater, R. Toth, E. Zeqiraj, D. R. Alessi, *EMBO J.* **2011**, *30*, 1730-1741.

[4] J. Boudeau, A. F. Baas, M. Deak, N. A. Morrice, A. Kieloch, M. Schutkowski, A. R. Prescott, H. C. Clevers, D. R. Alessi, *EMBO J.* **2003**, *22*, 5102-5114.

[5] T. M. Moon, F. Correa, L. N. Kinch, A. T. Piala, K. H. Gardner, E. J. Goldsmith, *J. Mol. Biol.* **2013**, *425*, 1245-1252.

[6] C. A. Taylor, M. H. Cobb, *Molecular Pharmacol.* **2021**, DOI: 10.1124/molpharm.121.000307.

[7] F. H. Wilson, S. Disse-Nicodeme, K. A. Choate, K. Ishikawa, C. Nelson-Williams, I. Desitter, M. Gunel, D. V. Milford, G. W. Lipkin, J. M. Achard, M. P. Feely, B. Dussol, Y. Berland, R. J. Unwin, H. Mayan, D. B. Simon, Z. Farfel, X. Jeunemaitre, R. P. Lifton, *Science* **2001**, *293*, 1107-1112.

[8] a) A. Ohta, F. R. Schumacher, Y. Mehellou, C. Johnson, A. Knebel, T. J. Macartney, N. T. Wood, D. R. Alessi, T. Kurz, *Biochem. J.* **2013**, *451*, 111-122; b) M. Wakabayashi, T. Mori, K. Isobe, E. Sohara, K. Susa, Y. Araki, M. Chiga, E. Kikuchi, N. Nomura, Y. Mori, H. Matsuo, T. Murata, S. Nomura, T. Asano, H. Kawaguchi, S. Nonoyama, T. Rai, S. Sasaki, S. Uchida, *Cell Rep.* **2013**, *3*, 858-868; c) S. Shibata, J. Zhang, J. Puthumana, K. L. Stone, R. P. Lifton, *Proc. Nat. Acad. Sci. U.S.A.* **2013**, *110*, 7838-7843.

[9] a) H. Louis-Dit-Picard, J. Barc, D. Trujillano, S. Miserey-Lenkei, N. Bouatia-Naji, O. Pylypenko, G. Beaurain, A. Bonnefond, O. Sand, C. Simian, E. Vidal-Petiot, C. Soukaseum, C. Mandet, F. Broux, O. Chabre, M. Delahousse, V. Esnault, B. Fiquet, P. Houillier, C. I. Bagnis, J. Koenig, M. Konrad, P. Landais, C. Mourani, P. Niaudet, V. Probst, C. Thauvin, R. J. Unwin, S. D. Soroka, G. Ehret, S. Ossowski, M. Caulfield, P. Bruneval, X. Estivill, P. Froguel, J. Hadchouel, J. J. Schott, X. Jeunemaitre, *Nature Genet.* **2012**, *44*, 456-460; b) L. M. Boyden, M. Choi, K. A. Choate, C. J. Nelson-Williams, A. Farhi, H. R. Toka, I. R. Tikhonova, R. Bjornson, S. M. Mane, G. Colussi, M. Lebel, R. D. Gordon, B. A. Semmekrot, A. Poujol, M. J. Valimaki, M. E. De Ferrari, S. A. Sanjad, M. Gutkin, F. E. Karet, J. R. Tucci, J. R. Stockigt, K. M. Keppler-Noreuil, C. C. Porter, S. K. Anand, M. L. Whiteford, I. D. Davis, S. B. Dewar, A. Bettinelli, J. J. Fadrowski, C. W. Belsha, T. E. Hunley, R. D. Nelson, H. Trachtman, T. R. Cole, M. Pinsk, D. Bockenhauer, M. Shenoy, P. Vaidyanathan, J. W. Foreman, M. Rasoulpour, F. Thameem, H. Z. Al-Shahrouri, J. Radhakrishnan, A. G. Gharavi, B. Goilav, R. P. Lifton, *Nature* **2012**, *482*, 98-102.

[10] a) G. Begum, H. Yuan, K. T. Kahle, L. Li, S. Wang, Y. Shi, B. E. Shmukler, S. S. Yang, S. H. Lin, S. L. Alper, D. Sun, *Stroke* **2015**, *46*, 1956-1965; b) H. Zhao, R. Nepomuceno, X. Gao, L. M. Foley, S. Wang, G. Begum, W. Zhu, V. M. Pigott, L. M. Falgoust, K. T. Kahle, S. S. Yang, S. H. Lin, S. L. Alper, T. K. Hitchens, S. Hu, Z. Zhang, D. Sun, *J. Cereb. Blood Flow Metab.* **2017**, *37*, 550-563.

[11] a) Y. Li, L. Li, J. Qin, J. Wu, X. Dai, J. Xu, *Oncogene* **2021**, *40*, 68-84; b) Y. Li, J. Qin, J. Wu, X. Dai, J. Xu, *Breast Cancer Res. Treat.* **2020**, *182*, 35-46.

[12] F. H. Rafiqi, A. M. Zuber, M. Glover, C. Richardson, S. Fleming, S. Jovanovic, A. Jovanovic, K. M. O'Shaughnessy, D. R. Alessi, *EMBO Mol. Med.* **2010**, *2*, 63-75.

[13] J. Zhang, M. I. H. Bhuiyan, T. Zhang, J. K. Karimy, Z. Wu, V. M. Fiesler, J. Zhang, H. Huang, M. N. Hasan, A. E. Skrzypiec, M. Mucha, D. Duran, W. Huang, R. Pawlak, L. M. Foley, T. K. Hitchens, M. B. Minnigh, S. M. Poloyac, S. L. Alper, B. J. Molyneaux, A. J. Trevelyan, K. T. Kahle, D. Sun, X. Deng, *Nature Commun.* **2020**, *11*, 78.

[14] a) K. Yamada, H. M. Park, D. F. Rigel, K. DiPetrillo, E. J. Whalen, A. Anisowicz, M. Beil, J. Berstler, C. E. Brocklehurst, D. A. Burdick, S. L. Caplan, M. P. Capparelli, G. Chen, W. Chen, B. Dale, L. Deng, F. Fu, N. Hamamatsu, K. Harasaki, T. Herr, P. Hoffmann, Q. Y. Hu, W. J. Huang, N. Idamakanti, H. Imase, Y. Iwaki, M. Jain, J. Jeyaseelan, M. Kato, V. K. Kaushik, D. Kohls, V. Kunjathoor, D. LaSala, J. Lee, J. Liu, Y. Luo, F. Ma, R. Mo, S. Mowbray, M. Mogi, F. Ossola, P. Pandey, S. J. Patel, S. Raghavan, B. Salem, Y. H. Shanado, G. M. Trakshel, G. Turner, H. Wakai, C. Wang, S. Weldon, J. B. Wielicki, X. Xie, L. Xu, Y. I. Yagi, K. Yasoshima, J. Yin, D. Yowe, J. H. Zhang, G. Zheng, L. Monovich, *Nature Chem. Biol.* **2016**, *12*, 896-898; b) K. Yamada, J. H. Zhang, X. Xie, J. Reinhardt, A. Q. Xie, D. LaSala, D. Kohls, D. Yowe, D. Burdick, H. Yoshisue, H. Wakai, I. Schmidt, J. Gunawan, K. Yasoshima, Q. K. Yue, M. Kato, M. Mogi, N. Idamakanti, N. Kreder, P. Drueckes, P. Pandey, T. Kawanami, W. Huang, Y. I. Yagi, Z. Deng, H. M. Park, *ACS Chem. Biol.* **2016**, *11*, 3338-3346; c) K. Yamada, J. Levell, T. Yoon, D. Kohls, D. Yowe, D. F. Rigel, H. Imase, J. Yuan, K. Yasoshima, K. DiPetrillo, L. Monovich, L. Xu, M. Zhu, M. Kato, M. Jain, N. Idamakanti, P. Taslimi, T. Kawanami, U. A. Argikar, V. Kunjathoor, X. Xie, Y. I. Yagi, Y. Iwaki, Z. Robinson, H. M. Park, *J. Med. Chem.* **2017**, *60*, 7099-7107.

[15] a) M. A. AlAmri, H. Kadri, L. J. Alderwick, N. S. Simpkins, Y. Mehellou, *ChemMedChem* **2017**, *12*, 639-645; b) E. Kikuchi, T. Mori, M. Zeniya, K. Isobe, M. Ishigami-Yuasa, S. Fujii, H. Kagechika, T. Ishihara, T. Mizushima, S. Sasaki, E. Sohara, T. Rai, S. Uchida, *J. Am. Soc. Nephrol.* **2015**, *26*, 1525-1536; c) T. Mori, E. Kikuchi, Y. Watanabe, S. Fujii, M. Ishigami-Yuasa, H. Kagechika, E. Sohara, T. Rai, S. Sasaki, S. Uchida, *Biochem. J.* **2013**, *455*, 339-345.

[16] J. Zhang, K. Siew, T. Macartney, K. M. O'Shaughnessy, D. R. Alessi, *Human Mol. Genet.* **2015**, *24*, 4545-4558.

[17] F. Villa, J. Goebel, F. H. Rafiqi, M. Deak, J. Thastrup, D. R. Alessi, D. M. van Aalten, *EMBO Rep.* **2007**, *8*, 839-845.

[18] Y. Liu, D. Eisenberg, *Protein Sci.* **2002**, *11*, 1285-1299.

[19] A. C. Vitari, J. Thastrup, F. H. Rafiqi, M. Deak, N. A. Morrice, H. K. Karlsson, D. R. Alessi, *Biochem. J.* **2006**, *397*, 223-231.

[20] C. A. t. Taylor, S. W. An, S. G. Kankanamalage, S. Stippec, S. Earnest, A. T. Trivedi, J. Z. Yang, H. Mirzaei, C. L. Huang, M. H. Cobb, *Proc. Nat. Acad. Sci. U.S.A.* **2018**, *115*, 3840-3845.

[21] G. Winter, D. G. Waterman, J. M. Parkhurst, A. S. Brewster, R. J. Gildea, M. Gerstel, L. Fuentes-Montero, M. Vollmar, T. Michels-Clark, I. D. Young, N. K. Sauter, G. Evans, *Acta Crystallogr. D Struct. Biol.* **2018**, *74*, 85-97.

[22] G. Winter, C. M. Lobley, S. M. Prince, *Acta Crystallogr. D Biol. Crystallogr.* **2013**, *69*, 1260-1273.

[23] A. J. McCoy, *Methods Mol. Biol.* **2017**, *1607*, 421-453.

[24] O. Kovalevskiy, R. A. Nicholls, F. Long, A. Carlon, G. N. Murshudov, *Acta Crystallogr. D Struct. Biol.* **2018**, *74*, 215-227.

[25] P. D. Adams, P. V. Afonine, G. Bunkoczi, V. B. Chen, I. W. Davis, N. Echols, J. J. Headd, L. W. Hung, G. J. Kapral, R. W. Grosse-Kunstleve, A. J. McCoy, N. W. Moriarty, R. Oeffner, R. J. Read, D. C. Richardson, J. S. Richardson, T. C. Terwilliger, P. H. Zwart, *Acta Crystallogr. D. Biol. Crystallogr.* **2010**, *66*, 213-221.

[26] P. Emsley, B. Lohkamp, W. G. Scott, K. Cowtan, *Acta Crystallogr. D. Biol. Crystallogr.* **2010**, *66*, 486-501.

[27] C. Vonrhein, I. J. Tickle, C. Flensburg, P. Keller, W. Paciorek, A. Sharff, G. Bricogne, *Acta Crystallogr.* **2018**, *74*, a360-a360.

[28] W. Kabsch, C. Sander, *Biopolymers* **1983**, *22*, 2577-2637.

[29] W. G. Touw, C. Baakman, J. Black, T. A. te Beek, E. Krieger, R. P. Joosten, G. Vriend, *Nucleic Acids Res.* **2015**, *43*, D364-368.

[30] E. Krissinel, K. Henrick, *J. Mol. Biol.* **2007**, *372*, 774-797.

[31] N. Jiravanichanun, C. Hongo, G. Wu, K. Noguchi, K. Okuyama, N. Nishino, T. Silva, *ChemBioChem* **2005**, *6*, 1184-1187.

[32] Ö. Kartal, F. Andres, M. P. Lai, R. Nehme, K. Cottier, *SLAS Discov.* **2021**, 24725552211013827.

[33] M. A. Alamri, M. Jeeves, Y. Mehellou, *Biochem. Biophys. Res. Commun.* **2019**, *512*, 338-343.

Entry for the Table of Contents

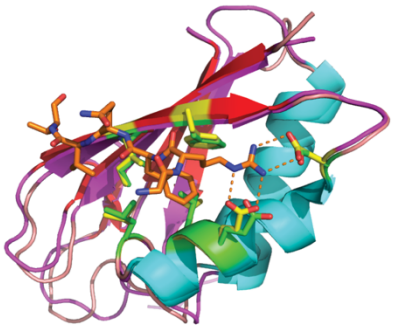

Human SPAK and OSR1 CCT domain structures

The inhibition of SPAK and OSR1 kinases binding to their upstream WNK kinases has been identified as a plausible strategy for inhibiting the WNK-activation of SPAK and OSR1 kinases. To facilitate the discovery of SPAK and OSR1 kinases inhibitors as potential therapeutics, we herein report the crystal structures of the highly conserved *C*-terminal domains of human SPAK and OSR1, which mediate the binding to, and activation, by their upstream WNK kinases.

Institute and/or researcher Twitter usernames: @Youcef_Mehellou, @PharmacyCU, @CUMedicinesInst.

SUPPORTING INFORMATION

CONTENTS

PDB code:	7o86 (SPAK-CCT)	7okw (OSR1-CCT)
Diffraction source	IO3 – Diamond Light Source	IO4 – Diamond Light Source
Wavelength	0.97628	0.97950
Resolution range	45.45 - 1.73 (1.792 - 1.73)	55.7-1.62 (1.764-1.62)
Space group	P 2_1 2_1 2_1	C2
Unit cell	39.61 50.55 103.80 90 90 90	70.17 49.42 56.44 90 99.44 90
Total reflections	293450 (28311)	132058 (6432)
Unique reflections	22482 (2168)	19062 (954)
Multiplicity	13.1 (12.8)	6.9 (6.7)
Completeness (%)	99.63 (97.88)	78.6 (17.9) (spherical) 91.5 (49.2) (ellipsoidal)
Mean I/sigma(I)	6.83 (0.43)	10.0 (1.4)
Wilson B-factor	25.83	21.04
R-merge	0.2553 (3.974)	0.114 (1.246)
R-meas	0.2657 (4.139)	0.123 (1.352)
R-pim	0.07308 (1.15)	0.047 (0.519)
CC1/2	0.997 (0.281)	0.999 (0.624)
Reflections used in refinement	22400 (2165)	19058 (360)
Reflections used for R-free	1100 (106)	930 (14)
R-work	0.1965 (0.3791)	0.1840 (0.3016)
R-free	0.2400 (0.3820)	0.2165 (0.2968)
CC(work)	0.950 (0.621)	0.967 (0.810)
CC(free)	0.958 (0.517)	0.913
Number of non-hydrogen atoms	1937	1733
macromolecules	1729	1532
ligands	4	21
solvent	204	180
Protein residues	191	194
RMS(bonds)	0.017	0.006
RMS(angles)	1.44	0.88
Ramachandran favored (%)	97.33	98.95
Ramachandran allowed (%)	2.14	1.05
Ramachandran outliers (%)	0.53	0.00
Rotamer outliers (%)	4.21	2.40
Clashscore	8.36	0.96
Average B-factor	34.40	25.71
macromolecules	33.58	24.55
ligands	51.69	46.03
solvent	41.04	33.24

Values in parentheses are for the outer shell. Note that the OSR1-CCT data were processed with STARANISO,[1] which processes data anisotropically.

Supporting Table S1. Data collection and refinement statistics.

Reference	Construct	Method	KD (and IC_{50} where indicated)
Vitari et al. 2006[2]	GST-OSR1 CCT (429-527) GST-OSR1 L437A	Biacore; immobilised biotinylated RFQV peptide	8 nM No binding
Villa et al. 2007[3]	GSR-OSR1 (434-527) GST-OSR1 L473A	Biacore; immobilised biotinylated RFQV peptide	Not cited. Fig 4A response units vs concentration No binding
Zhang et al. 2015[4]	GST-SPAK (452-545) GST-SPAK L491A	Fluorescence polarisation Lumino-Green-labelled WNK peptide	0.6 µM 88.2 µM
Mori et al. 2013[5]	Rat GST-SPAK (452-553)	Fluorescent TAMRA labelled RFQV-WNK4 RFQV-WNK1 NCC-RFTI AFQV-WNK4 Biacore; immobilised GST-SPAK with STOCK1S-50699 (PubChem-CID 5749625) GST-SPAK with STOCK2S-26016 (PubChem-CID3135086)	1.3 µM 1.3 µM 11.2 µM No binding 32 µM 20 µM
Ishigami-Yuasa et al. 2017[6]	Rat GST-SPAK (452-553)	Fluorescent TAMRA RFQV-WNK4 and various substitutions in lead compound 1 Compound 10 Compound 13 Compound 20	 15.4 µM IC_{50} 6.9 µM IC_{50} 2.6 µM IC_{50} 4.8 µM IC_{50}
Kikuchi et al. 2015[7]	GST-SPAK [T233E]	Biacore 1S-14279 binding and ELISA IC_{50} Closantel	KD not cited, IC_{50} 0.26 µM KD not cited, IC_{50} 0.77 µM
AlAmri et al. 2017[8]	GST-OSR1 (433-end)	Fluorescence polarisation RFQV-WNK4 peptide	 2.11 µM

	GST-OSR1 L473A (433-end)	RFQV-WNK4 peptide	13.17 µM
Taylor et al 2018[9]	His6-OSR CCT (433–527) His6-SPAK CCT (449–545)	Fluorescence anisotrophy FAM probe chimera of WNK4 and WNK1 R-F-x-V peptide with competing WNK1 Probe vs WNK1	5.1 ± 0.4 µM 2.6 ± 0.2 µM

Supporting Table S2. Literature reporting K_D or IC_{50} values by different methods to the RFVQ motif of either WNK4 or WNK1.

Ligand	Analyte (conc)	Ka M-1s-1	Kd s-1	KD µM	Rmax pg/mm2	Sqrt(chi2) pg/mm2
SPAK	18mer(2µM)	475783.2	0.567316	1.19	43.62	0.17
SPAK	18mer(5µM)	558691.7	0.613815	1.10	38.24	0.17
SPAK	18mer(10µM)	552270.2	0.6317	1.14	34.74	0.18
SPAK	18mer(20µM)	514495.5	0.705448	1.37	37.82	0.21
OSR	18mer(2uM)	119380.5	0.515295	4.32	158.96	0.17
OSR	18mer(5uM)	219859.4	0.560134	2.55	99.16	0.25
OSR	18mer(10uM)	245014.4	0.571064	2.33	85.41	0.27
OSR	18mer(20uM)	239972.6	0.618801	2.58	89.68	0.29

Supporting Table S3. Kinetic values for waveRAPID binding of the 18-mer peptide to SPAK and OSR1. Kinetic values for waveRAPID binding of the 18-mer peptide SEEGKPQLVGRFQVTSSK (analyte) at 2, 5, 10 and 20 µM, to immobilized biotin-OSR1 and biotin-SPAK on the Creoptix WAVE (see supplementary Figures 5 and 6 for raw data). Ka = association rate, kd = dissociation rate, K_D = dissociation rate constant, Rmax = the maximum signal generated by an interaction between a ligand – analyte in pg/mm^2.

A

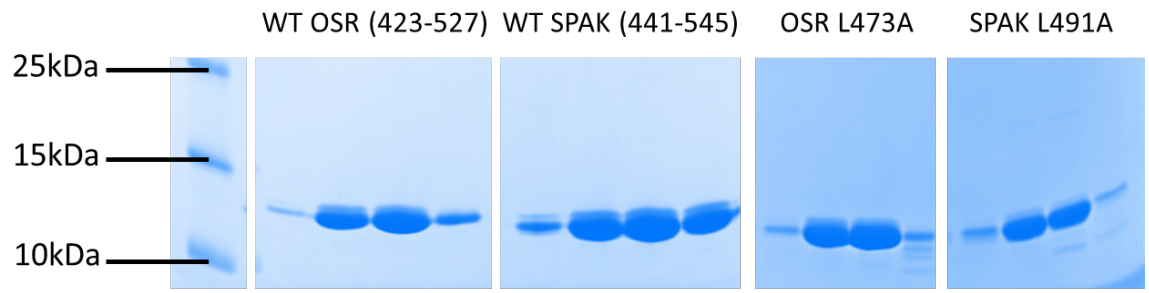

B

Supporting Figure S1. SDS PAGE gels of purified of SPAK and OSR1. A. SDS PAGE using 16% Tris Tricine gels of wild type human SPAK CCT, OSR1 CCT, SPAK [L491A] and OSR [L473A] after final size exclusion. The fractions for each were pooled and concentrated. Concentrated protein was either cleaved with TEV protease for crystallisation or uncleaved protein was biotinylated with BirA ligase for binding kinetics. Marker molecular weights are indicated in kD. **B**. Crystal of human SPAK from Morpheus screen A5 grown at 6°C.

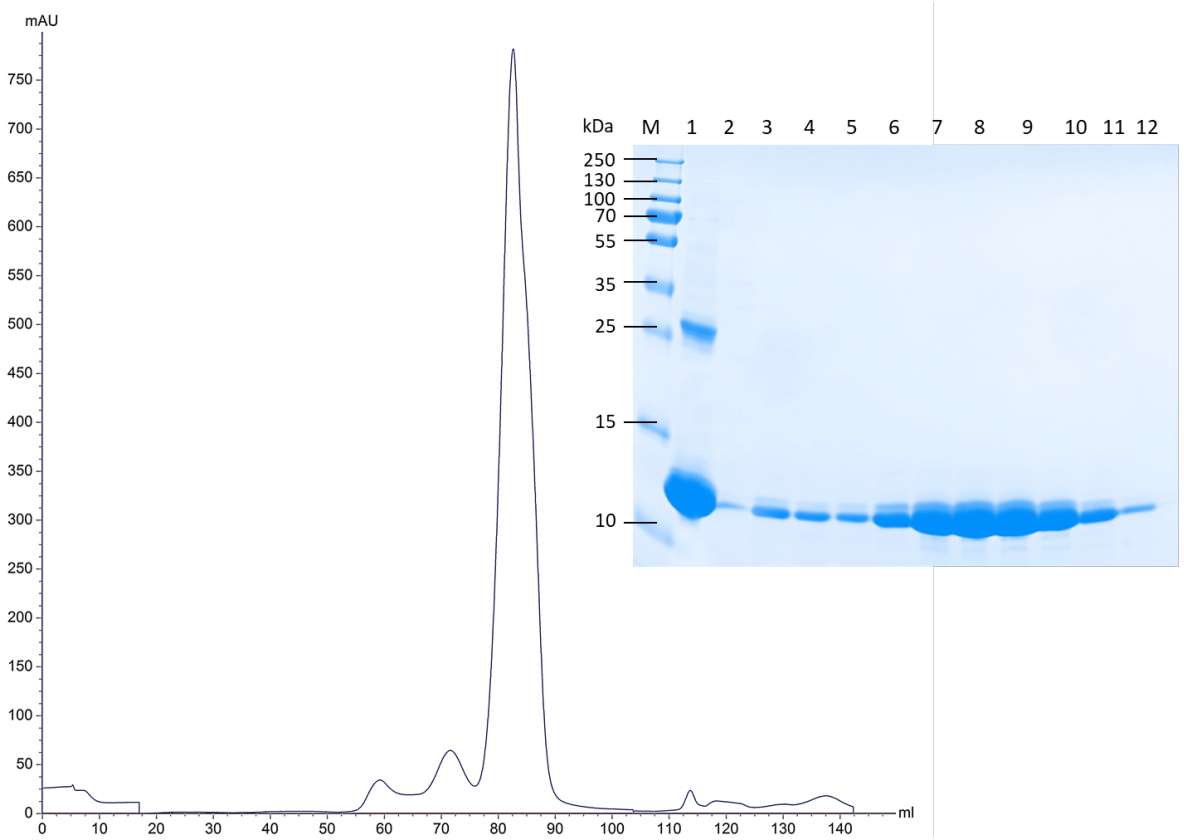

Supporting Figure S2. Size-exclusion chromatography elution profile of uncleaved SPAK CCT with inset showing a 16% SDS-PAGE analysis of the peaks. 'M' is protein markers. Lane 1 is the concentrated protein after HisTrap purification; Lanes 2 and 3 a fraction from each of the smaller peaks preceding the main peak. Lanes 4-12 protein contained in the fractions over the major peak. These were pooled and concentrated for cleavage for crystallography.

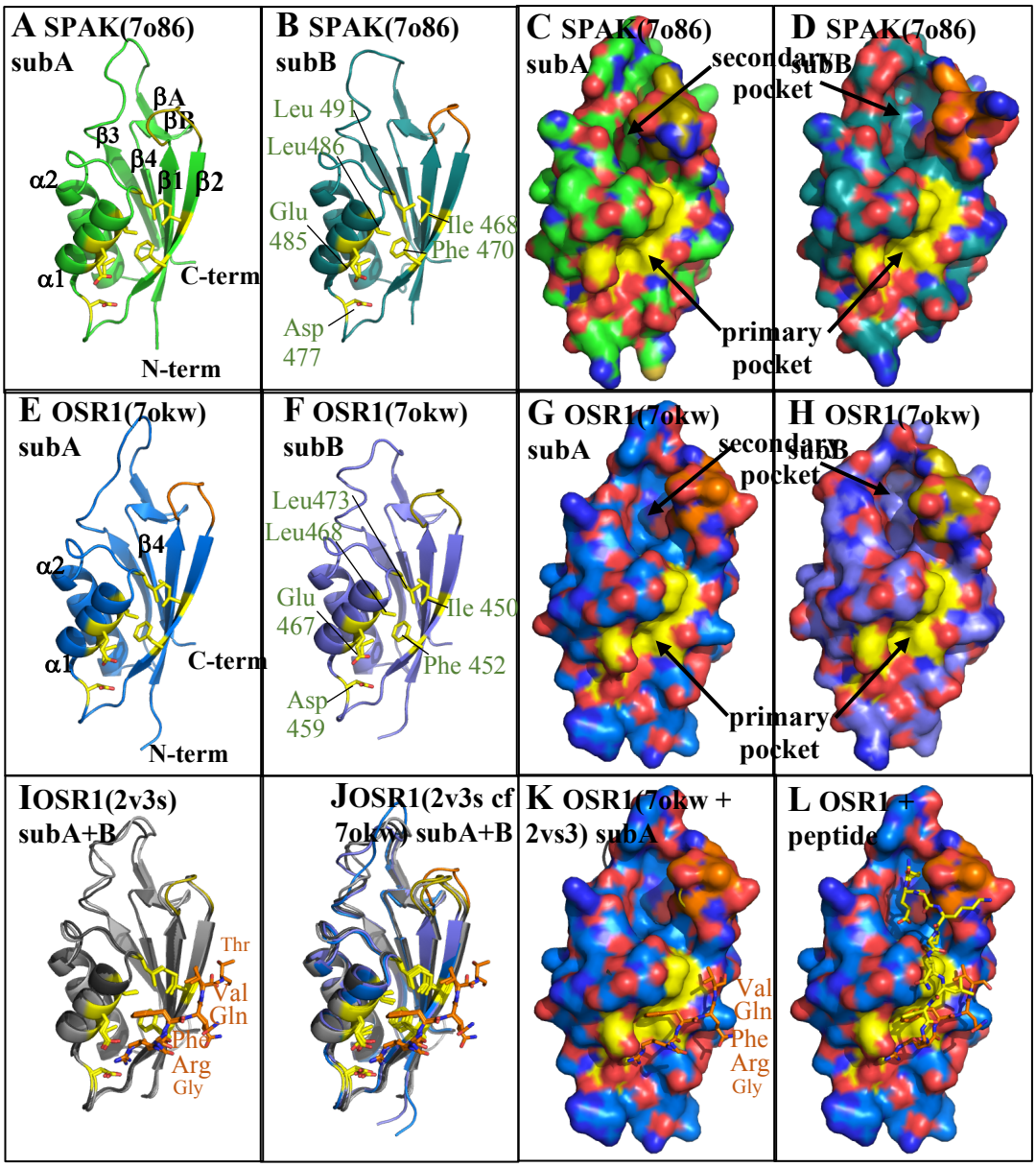

Supporting Figure S3. hSPAK and hOSR1 CCT domains crystal structures. **A,B**. The A and B subunits from the 1.73Å structure of hSPAK1 CCT domain (pdb code: 7o86) are shown in cartoon. Seven residues in the primary binding are shown as sticks with yellow carbons. **C,D**. Surface views of the same structures. Note the carbons in the loop between the b1 and b2 strands are colored differently. **EF** and **GH** Equivalent views of the A and B subunits in the 1.62Å hOSR1 structure (PDB code 7okw). **I** The A and B subunits from the 1.70Å (PDB code 2v3s) structure of OSR1 with a peptide (GRFQVT; orange carbons –sticks) are shown superposed. The seven residues Ile 450, Phe 452, Asp 459, Val 464, Glu 467, Leu 468 and Leu 473 are shown as sticks with yellow carbons. **J** The two subunits from the 1.62Å hOSR1 structure (PDB code 7okw) are shown superposed on the two subunits from the 1.70Å structure of OSR1 with a peptide. **K**. The surface of subunit A from the apo 1.62Å hOSR1 structure is shown with 5mer peptide from subunit A from the 1.70Å structure of OSR1 with a peptide superposed (C-terminal Thr is not seen). **L** The *N*-terminal residues (**EEGKPQLV** – yellow carbons) from the 18mer WNK4 peptide have been modelled on as a polyproline helix occupying the secondary pocket and packing against the F and V motif from the GRFQV (orange carbons) (see Experimental section for details). The 18mer WNK4 peptide is S***EEGKPQLV***GRFQVTSSK.

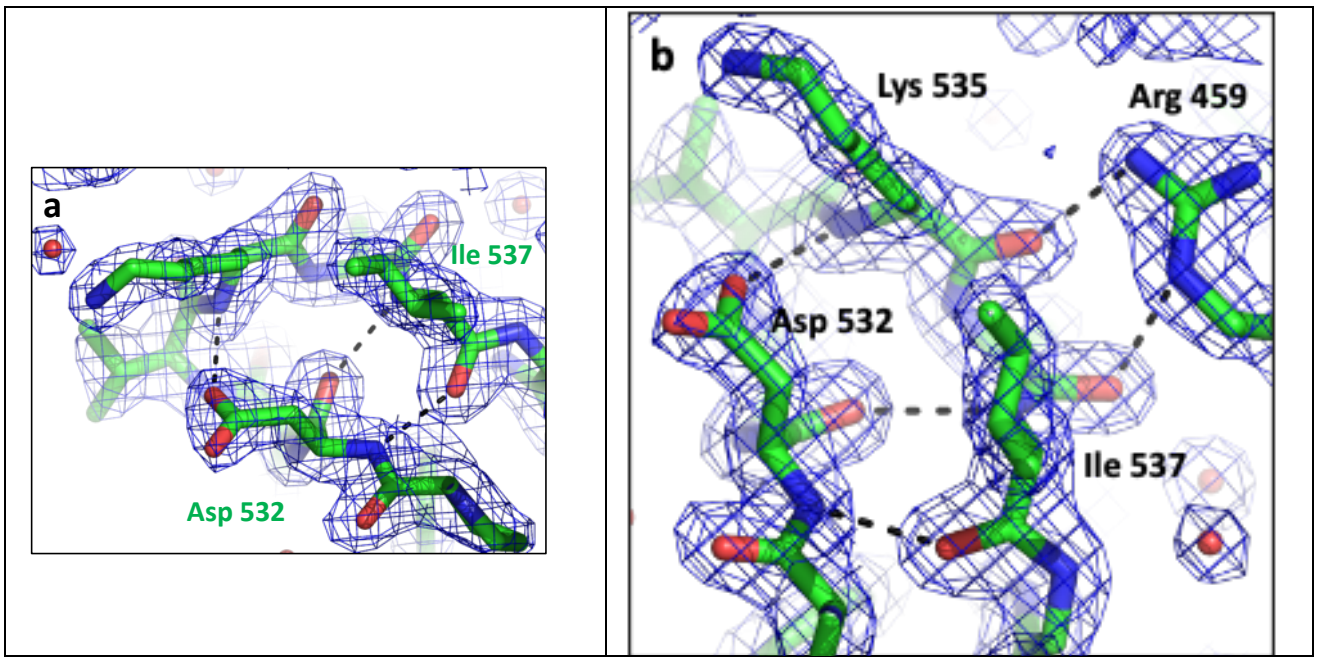

Supporting Figure S4. Electron density maps of the b-bridge between Asp 532 (D532) and Ile 537 (I537) in hSPAK. **A**. The final 2fo-fc map (contoured at 1.4sigma) around Asp 532 (D532) and Ile 537 (I537) from the 1.73Å hSPAK structure. Dotted black lines are hydrogen bonds from involving Asp 532 (D532). **B**. An alternative view at 1.5sigma, showing hydrogen bonds to the side-chain of Arg 459 (R459), the C-terminal residue of the first β-strand (β1).

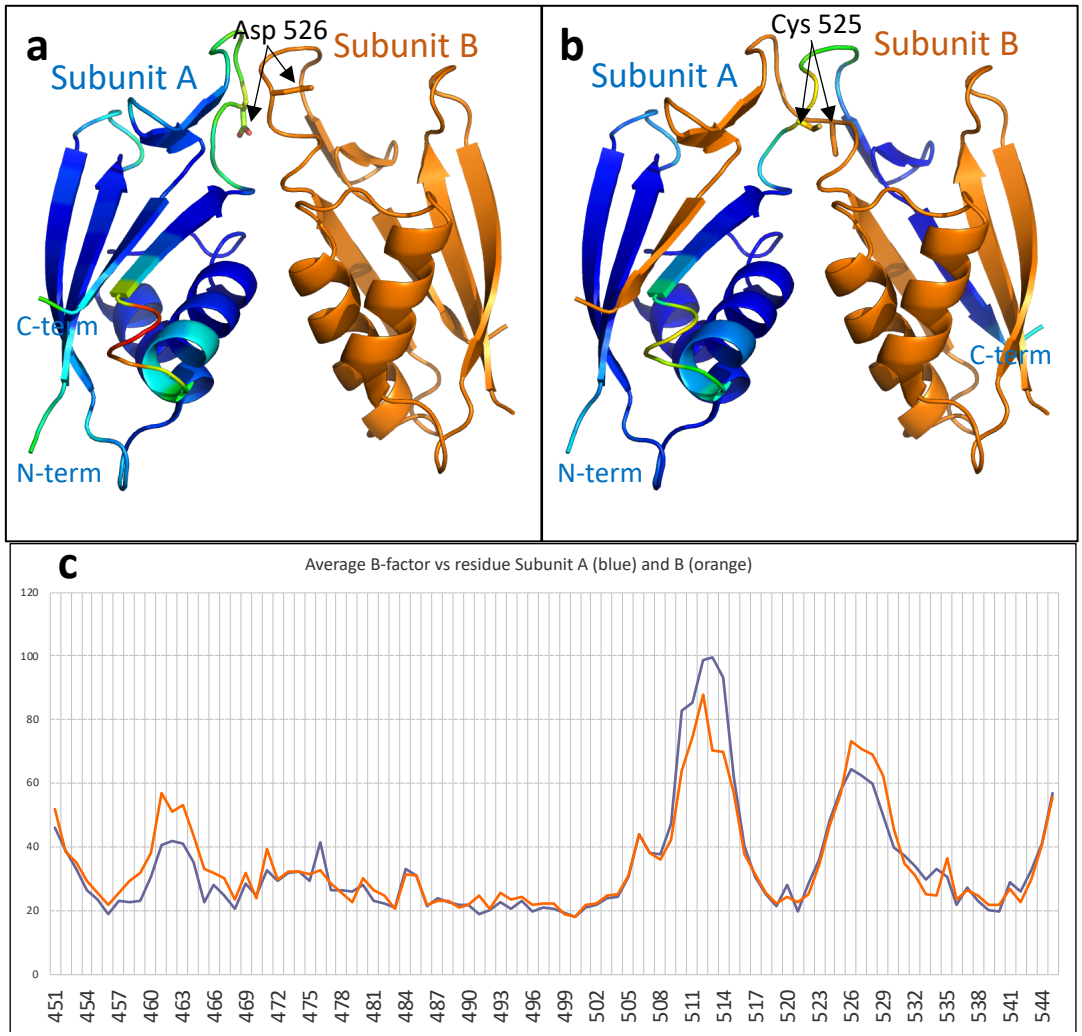

Supporting Figure S5. A model of a strand exchanged dimer in the 1.73Å hSPAK CCT domain structure. A. 1.73Å structure of hSPAK1 (pdb code: 7o86) is shown as a cartoon. Subunit A is coloured by temperature factor (blue – cold, yellow – warm, red – hot). Subunit B is coloured orange. Side-chains of residue Asp 526 (D526) are shown on each subunit. **B**. An alternatively refined 'domain swapped' dimer of the same structure. Side-chains of Cys 525 (C525) are shown on each subunit. **C.** Average B factor versus residue number plot with subunit A shown by blue line and subunit B by orange line.

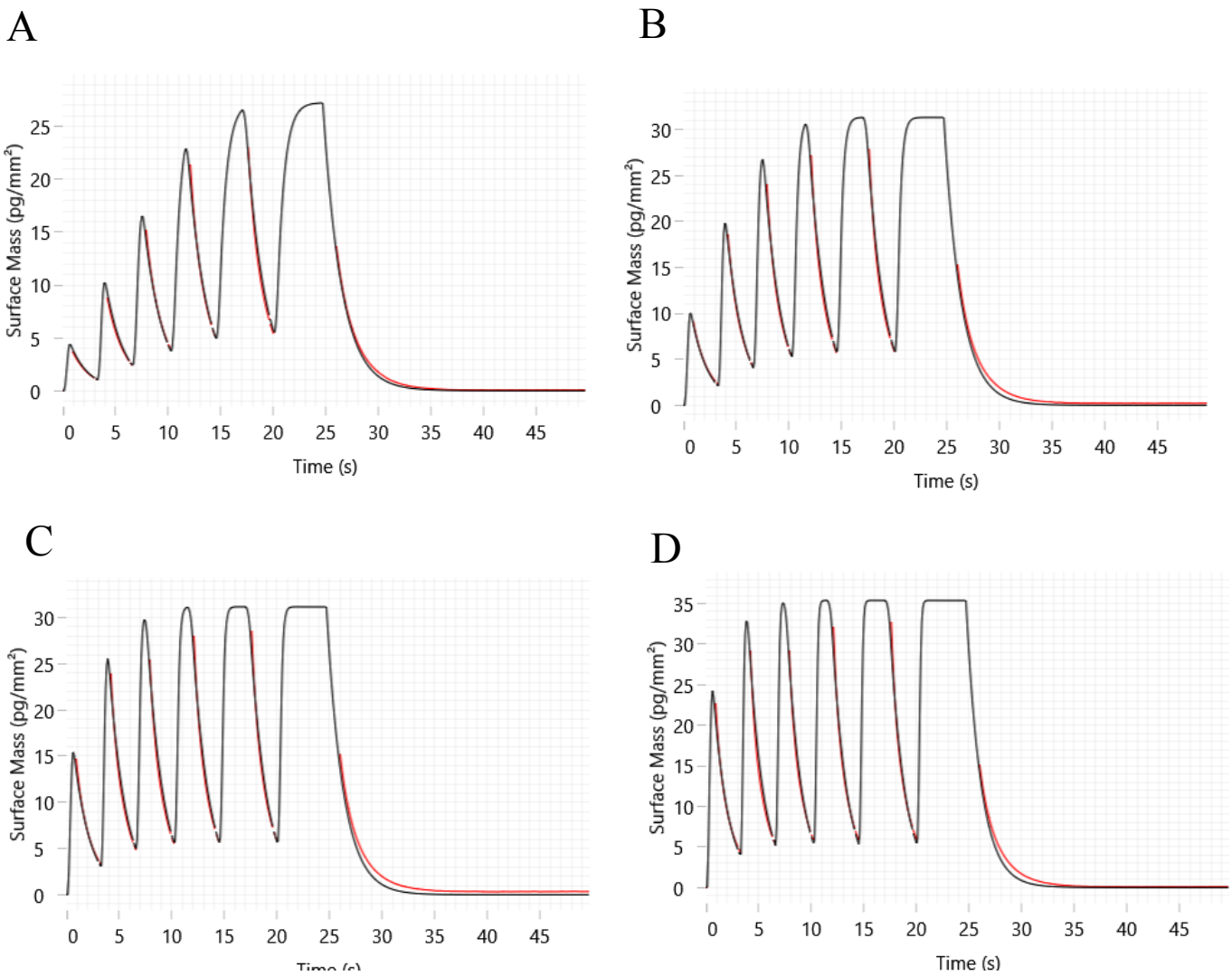

Supporting Figure S6. Binding of 18-mer peptide to SPAK on the WAVE. WaveRAPID kinetics. Binding was measured for the 18-mer peptide SEEGKPQLVGRFQVTSSK (analyte) at (**A**) 2 µM, (**B**) 5 µM, (**C**) 10 µM and (**D**) 20 µM to immobilized biotin-SPAK. The double-referenced response data (red) are fitted with a one-to-one binding model (black lines) in waveControl (see Supplementary Table 3 for derived kinetics values).

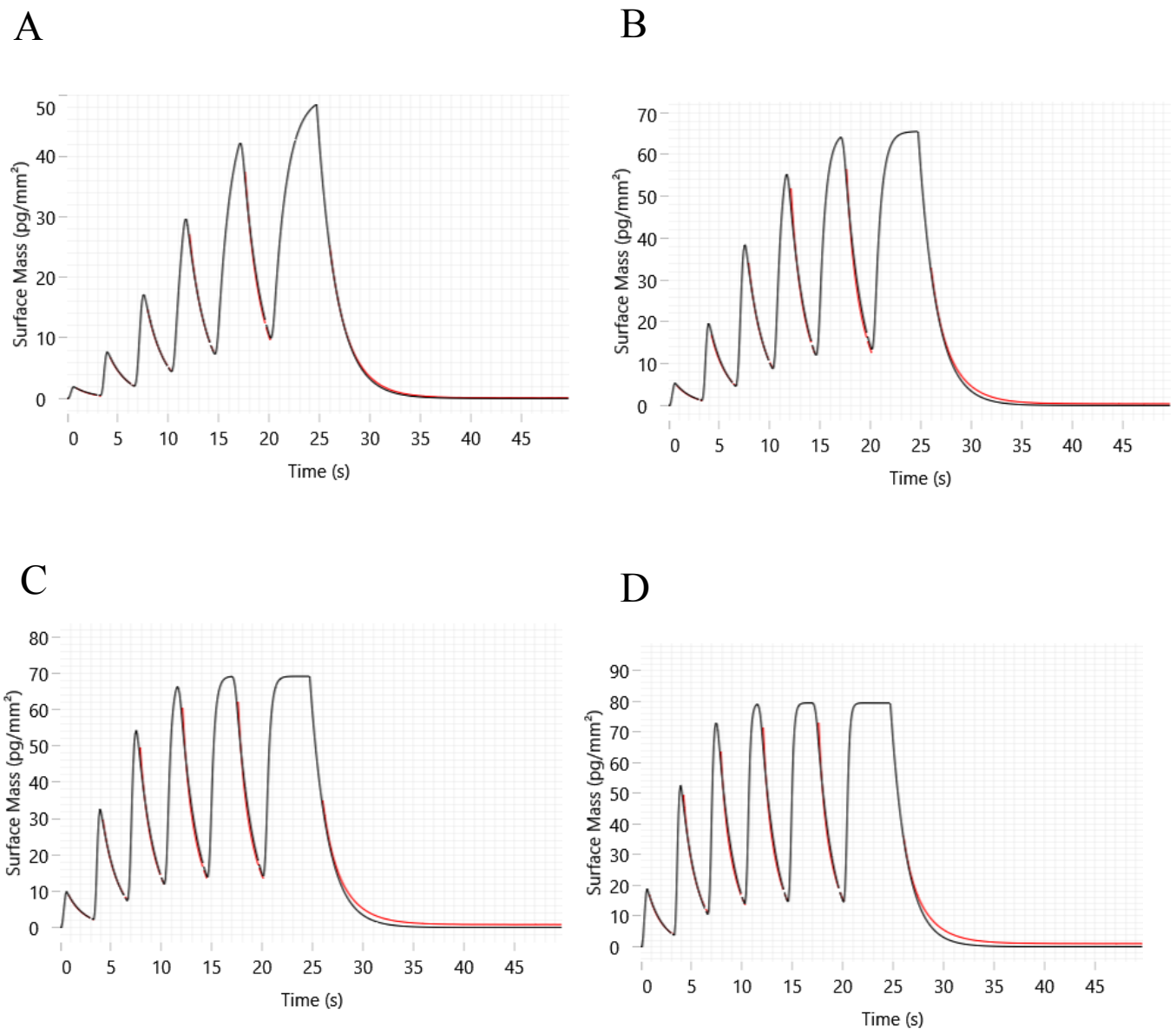

Supporting Figure S7. Binding of 18-mer peptide to OSR1 on the WAVE. WaveRAPID kinetics. Binding was measured for the 18-mer peptide SEEGKPQLVGRFQVTSSK (analyte) at (**A**) 2 µM, (**B**) 5 µM, (**C**) 10 µM and (**D**) 20 µM to immobilized biotin-OSR1. The double-referenced response data (red) were fitted with a one-to-one binding (black lines) with a suitable model in waveControl (see Supplementary Table 3 for derived kinetics values).

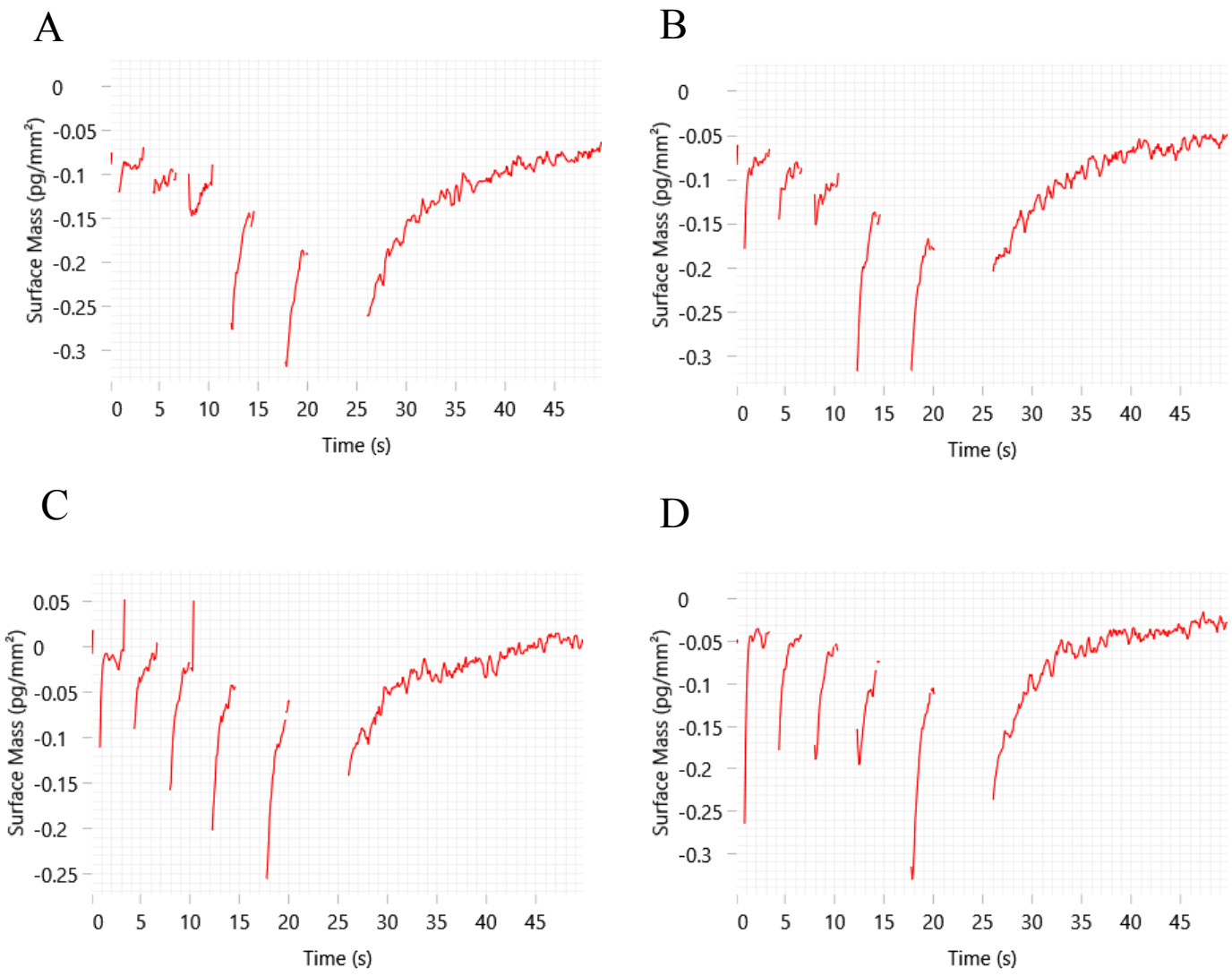

Supporting Figure S8. No binding of 18-mer peptide to SPAK L491A on the WAVE. WaveRAPID kinetics. Binding was measured for the 18-mer peptide SEEGKPQLVGRFQVTSSK (analyte) at (**A**) 2 µM, (**B**) 5 µM, (**C**) 10 µM and (**D**) 20 µM to immobilized biotin-SPAK L491A. The double-referenced response data (red) could noto be fitted with a suitable model in waveControl. Binding is not observed indicated by the high association and dissociation errors and no Rmax. Compare with supplementary Figure 5 - for binding of peptide to wild-type SPAK.

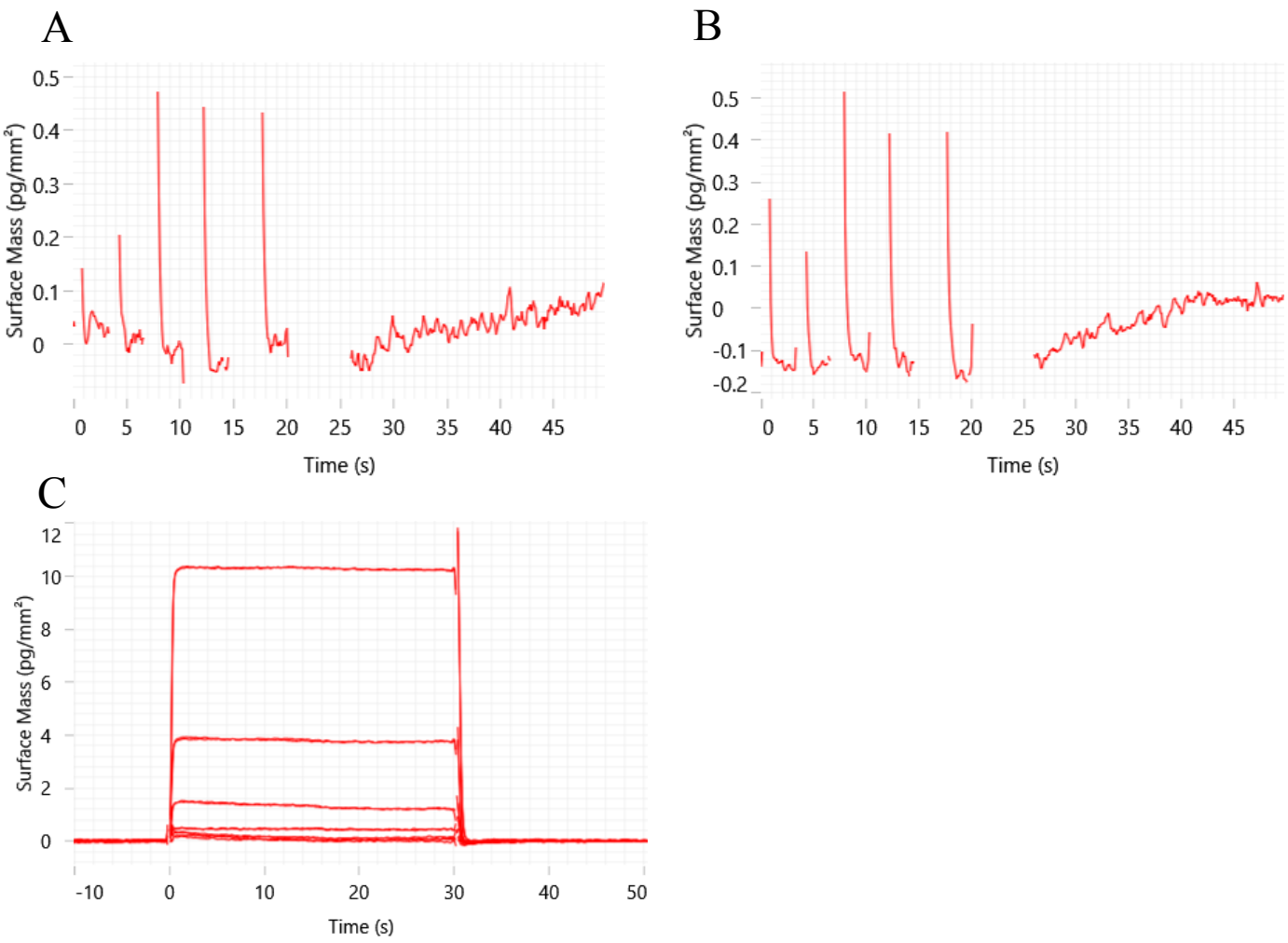

Supporting Figure S9. No binding of 18-mer peptide to OSR1 L473A on the WAVE. Raw data for binding of the 18-mer peptide SEEGKPQLVGRFQVTSSK (analyte) at (**A**) 10µM, (**B**) 20µM, to immobilized biotin-OSR1 L473A. (**C**) Multicylce kinetics for (50 µM, 17 µM, 5.5 µM, 1.8 µM, 0.6 µM, 0.2 µM) 18-mer peptide binding to OSR1 L473A. The double-referenced response data (red) could not be fitted with a one-to-one binding with a suitable model in waveControl. Binding is not observed indicated by the high association and dissociation errors and no Rmax. Compare with Supplementary Figure 6 for binding of 18-mer peptide to wild-type OSR1.

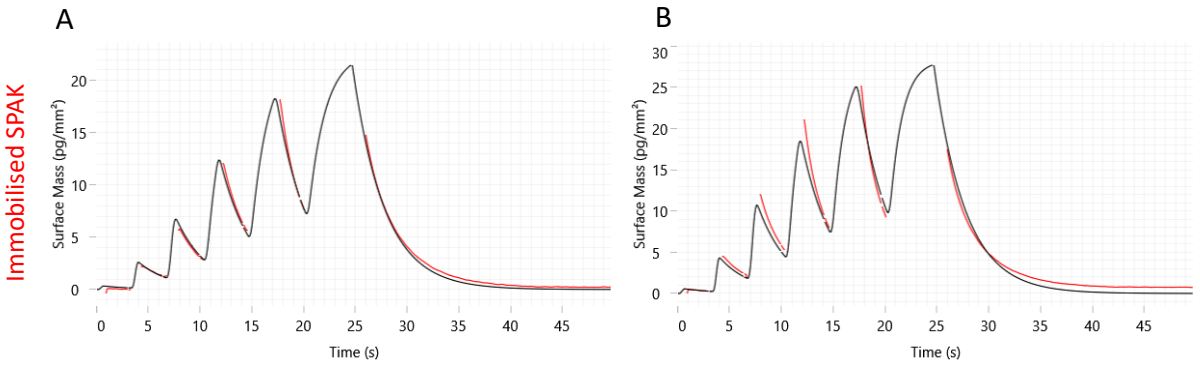

waveRAPID kinetics parameters		
Rmax	47.59	pg/mm^2
ka	5.946E4	M^{-1}s^{-1}
kd	3.27E-1	s^{-1}
K_D	5.5	µM

waveRAPID kinetics parameters		
Rmax	46.41	pg/mm^2
ka	5.177E4	M^{-1}s^{-1}
kd	3.319E-1	s^{-1}
K_D	6.411	µM

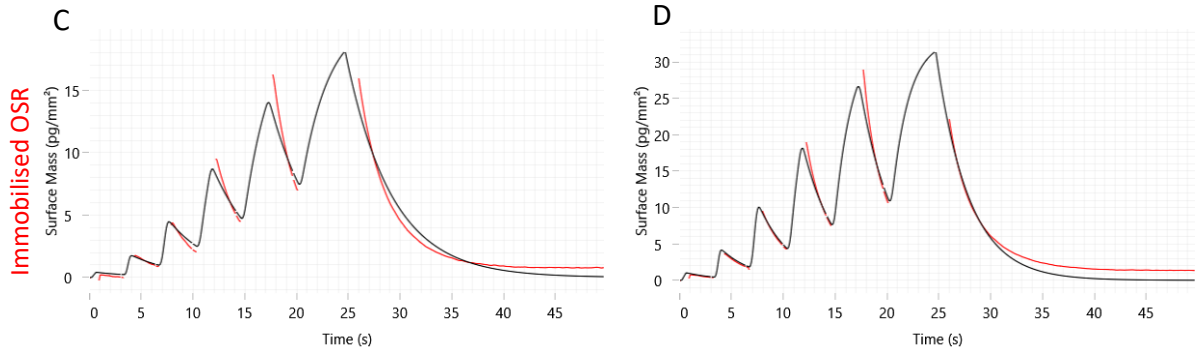

waveRAPID kinetics parameters		
Rmax	51.93	pg/mm^2
ka	3.04E4	M^{-1}s^{-1}
kd	2.26E-1	s^{-1}
K_D	7.427	µM

waveRAPID kinetics parameters		
Rmax	69.44	pg/mm^2
ka	2.92E4	M^{-1}s^{-1}
kd	3.19E-1	s^{-1}
K_D	10.947	µM

Supporting Figure S10. Binding of human NKCC1-derived 19-mer peptide to hSPAK and hOST1 OSR1 CCT domains on the WAVE. Binding was measured for the 19-mer peptide LGPTPSQSRFQVDLVSENA (analyte) to immobilized biotin-SPAK (A) peptide at 5µM and (B) peptide at 10µM or biotin-OSR (C) peptide at 5µM and (D) peptide at 10µM using waveRAPID. The double-referenced response data (red) are fitted with a one-to-one binding (black lines) with a suitable model in waveControl. Table summaries of kinetic parameters are shown: Rmax, *ka*, association rate constant; *kd*, dissociation rate constant; and K_D dissociation constant.

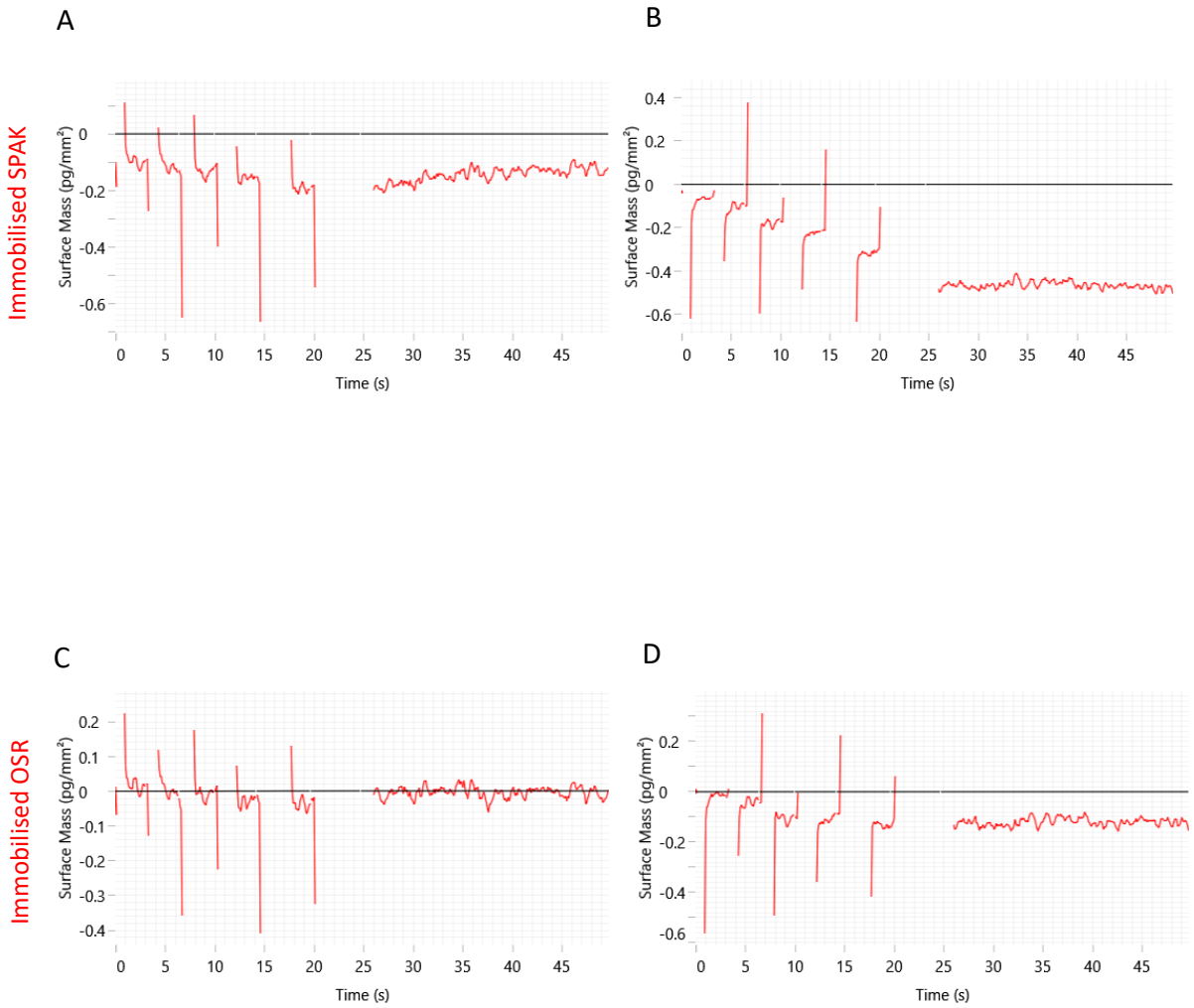

Supporting Figure S11. No binding of the human NKCC1-derived 19-mer peptide mutant to hSPAK and hOSR1 on the WAVE. Binding was measured for the 19-mer peptide LGPTPSQS**A**FQVDLVSENA (analyte) to immobilized biotin-SPAK (A) peptide at 5µM and (B) peptide at 10µM or biotin-OSR (C) peptide at 5µM and (D) peptide at 10µM using waveRAPID. There is clearly no binding of the mutated peptide to either SPAK or OSR.

References

[1] C. Vonrhein, I. J. Tickle, C. Flensburg, P. Keller, W. Paciorek, A. Sharff, G. Bricogne, *Acta Crystallogr.* **2018**, *74*, a360-a360.

[2] A. C. Vitari, J. Thastrup, F. H. Rafiqi, M. Deak, N. A. Morrice, H. K. Karlsson, D. R. Alessi, *Biochem. J.* **2006**, *397*, 223-231.

[3] F. Villa, J. Goebel, F. H. Rafiqi, M. Deak, J. Thastrup, D. R. Alessi, D. M. van Aalten, *EMBO Rep.* **2007**, *8*, 839-845.

[4] J. Zhang, K. Siew, T. Macartney, K. M. O'Shaughnessy, D. R. Alessi, *Human Mol. Genet.* **2015**, *24*, 4545-4558.

[5] T. Mori, E. Kikuchi, Y. Watanabe, S. Fujii, M. Ishigami-Yuasa, H. Kagechika, E. Sohara, T. Rai, S. Sasaki, S. Uchida, *Biochem. J.* **2013**, *455*, 339-345.

[6] M. Ishigami-Yuasa, Y. Watanabe, T. Mori, H. Masuno, S. Fujii, E. Kikuchi, S. Uchida, H. Kagechika, *Bioorg. Med. Chem.* **2017**, *25*, 3845-3852.

[7] E. Kikuchi, T. Mori, M. Zeniya, K. Isobe, M. Ishigami-Yuasa, S. Fujii, H. Kagechika, T. Ishihara, T. Mizushima, S. Sasaki, E. Sohara, T. Rai, S. Uchida, *J. Am. Soc. Nephrol.* **2015**, *26*, 1525-1536.

[8] M. A. AlAmri, H. Kadri, L. J. Alderwick, N. S. Simpkins, Y. Mehellou, *ChemMedChem* **2017**, *12*, 639-645.

[9] C. A. t. Taylor, S. W. An, S. G. Kankanamalage, S. Stippec, S. Earnest, A. T. Trivedi, J. Z. Yang, H. Mirzaei, C. L. Huang, M. H. Cobb, *Proc. Nat. Acad. Sci. U.S.A.* **2018**, *115*, 3840-3845.